has been serotyping based on the OSE residue of its GPL, the complete structures of only 15 GPLs have been defined. In addition to the chemical structures of various GPLs, genes encoding the glycosylation pathways in the biosynthesis of GPL have been identified and characterized (12, 21, 31). Epidemiological studies have shown that MAC serotypes 4 and 8 are the most frequently isolated from patients, and MAC serotype 16 is one of the next most common groups (32, 40). It has been suggested that the serotypes of MAC isolates participate in their virulence (29), and thus, understanding of the structure-pathogenicity relationship of GPLs is necessary. In the present study, we demonstrate the complete OSE structure of the GPL derived from serotype 16 MAC (*M. intracellulare*), which has a unique terminal-acylated-amido sugar, and we characterized the serotype 16 GPL-specific gene cluster involved in the glycosylation of carbohydrates.

MATERIALS AND METHODS

Bacterial strains and preparation of GPL. *M. intracellulare* serotype 16 strain ATCC 13950^T (NF 115) was purchased from the American Type Culture Collection (Manassas, VA). Three clinical isolates of *M. intracellulare* serotype 16 (NF 116 and 117) and *M. avium* serotype 1 (NF 113) were maintained in The Research Institute of Tuberculosis, Japan Anti-Tuberculosis Association. The preparation of GPL was performed as described previously (18, 24, 26). Briefly, each strain of *M. intracellulare* serotype 16 was grown in Middlebrook 7H9 broth (Difco Laboratories, Detroit, MI) with 0.5% glycerol and 10% Middlebrook oleic acid-albumin-dextrose-catalase enrichment (Difco) at 37°C for 2 to 3 weeks. The heat-killed bacteria were sonicated, and crude lipids were extracted with chloroform-methanol (2:1, vol/vol). The extracted lipids were dried and hydrolyzed with 0.2 N sodium hydroxide in methanol at 37°C for 2 h. After neutralization with 6 N hydrochloric acid, alkaline-stable lipids were partitioned by a two-layer system of chloroform-methanol (2:1, vol/vol) and water. The organic phase was recovered, evaporated, and precipitated with acetone to remove any acetone-insoluble components containing phospholipids and glycolipids. The supernatant was collected by centrifugation, dried, and then treated with a Sep-Pak silica cartridge (Waters Corporation, Milford, MA) with washing (chloroform-methanol, 95:5, vol/vol) and elution (chloroform-methanol, 1:1, vol/vol) for partial purification. GPL was completely purified by preparative thin-layer chromatography (TLC) of Silica Gel G (20 by 20 cm, 250 μm; Uniplate; Analtech, Inc., Newark, DE). The TLC plate was repeatedly developed with chloroform-methanol-water (65:25:4 and 60:16:2, vol/vol/vol) until a single spot was obtained. After exposure of the TLC plate to iodine vapor, the GPL band was marked, and then, the silica gels were scraped off and the GPL was eluted with chloroform-methanol (2:1, vol/vol).

Preparation of OSE moiety. β elimination of GPL was performed with alkaline borohydride, and the OSE elongated from D-*allo*-Thr was released as described previously (18, 24). Briefly, the GPL was dissolved in ethanol, and an equal volume of 10 mg/ml sodium borohydride or borodeuteride in 0.5 N sodium hydroxide was added and then stirred at 60°C for 16 h. The reaction mixture was decationized with Dowex 50W-X8 beads (Dow Chemical Company, Midland, MI), collected, and evaporated under nitrogen to remove boric acid. The dried residue was partitioned in two layers of chloroform-methanol (2:1, vol/vol) and water. The upper aqueous phase was recovered and evaporated. In these processes, the serotype 16-specific OSE was purified as an oligoglycosyl alditol.

MALDI-TOF and MALDI-TOF/TOF MS analyses. The molecular species of the intact GPL was detected by matrix-assisted laser desorption ionization–time of flight mass spectrometry (MALDI-TOF MS) with an Ultraflex II (Bruker Daltonics, Billerica, MA). The GPL was dissolved in chloroform-methanol (2:1, vol/vol) at a concentration of 1 mg/ml, and 1 μl was applied directly to the sample plate, and then 1 μl of 10 mg/ml 2,5-dihydroxybenzoic acid in chloroform-methanol (1:1, vol/vol) was added as a matrix. The intact GPL was analyzed in the reflectron mode with an accelerating voltage operating in a positive mode of 20 kV (5). Then the fragment pattern of the OSE was analyzed with MALDI-TOF/TOF MS. The OSE was dissolved in ethanol-water (3:7, vol/vol), and the matrix was 10 mg/ml 2,5-dihydroxybenzoic acid in ethanol-water (3:7, vol/vol). The OSE and the matrix were applied to the sample plate according to the method for intact GPL and analyzed in the lift-lift mode.

GC and GC-MS analyses of carbohydrates and *N*-acylated short-chain fatty acid. To determine the glycosyl composition and linkage position, gas chromatography (GC) and GC-MS analyses of partially methylated alditol acetate derivatives were performed. Perdeuteromethylation was conducted by the modified procedure of Hakomori as described previously (18, 20). Briefly, the dried OSE was dissolved with a mixture of dimethyl sulfoxide and sodium hydroxide, and deuteromethyl iodide was added. The reaction mixture was stirred at room temperature for 15 min and then water and chloroform were added. The chloroform-containing perdeuteromethylated OSE layer was collected, washed with water two times, and then completely evaporated. Partially deuteromethylated alditol acetates were prepared from perdeuteromethylated OSE by hydrolysis with 2 N trifluoroacetic acid at 120°C for 2 h, reduction with 10 mg/ml sodium borodeuteride at 25°C for 2 h, and acetylation with acetic anhydride at 100°C for 1 h (8, 18, 25). To identify amino-linked fatty acids, acidic methanolysis of serotype 16 GPL was performed with 1.25 M hydrogen chloride in methanol (Sigma-Aldrich, St. Louis, MO) at 100°C for 90 min, and the fatty acid methyl esters were extracted with *n*-hexane under the cooled ice. GC was performed using a 5890 series II gas chromatograph (Hewlett Packard, Avondale, PA) equipped with a fused SPB-1 capillary column (30 m, 0.25-mm inner diameter; Supelco Inc., Bellefonte, PA). Helium was used for electron impact (EI)-MS and isobutane for chemical ionization (CI)-MS as a carrier gas. A JMS SX102A double-focusing mass spectrometer (JEOL, Tokyo, Japan) was connected to the gas chromatograph as a mass detector. The molecular separator and the ion source energy were 70 eV for EI and 30 eV for CI, and the accelerating voltage was 8 kV. The D and L configurations of Rha residues were determined by comparative GC-MS analysis of trimethylsilylated (*S*)-(+)-sec-butyl glycosides and (*R*)-(−)-sec-butyl glycosides prepared from an authentic standard L-Rha (19).

NMR analysis of GPL. The GPL was dissolved in chloroform-d ($CDCl_3$)-methanol-d_4 (CD_3OD) (2:1, vol/vol). To define the anomeric configurations of each glycosyl residue, ^1H and ^{13}C nuclear magnetic resonance (NMR) was employed. Both homonuclear correlation spectrometry (COSY) and ^1H-detected [^1H, ^{13}C] heteronuclear multiple-quantum correlation (HMQC) were recorded with a Bruker Avance-600 (Bruker BioSpin Corp., Billerica, MA), as described previously (9, 18, 24, 34).

Construction of *M. intracellulare* serotype 16 cosmid library. A cosmid library of *M. intracellulare* serotype 16 strain ATCC 13950^T was constructed as described previously (18). Bacterial cells were disrupted mechanically, and genomic DNA was extracted with phenol-chloroform and then precipitated with ethanol. Genomic DNA randomly sheared into 30- to 50-kb fragments in the extraction process was fractionated and electroeluted from agarose gels using a Takara Recochip (Takara, Kyoto, Japan). These DNA fragments were rendered blunt ended using T4 DNA polymerase and deoxynucleoside triphosphates and then were ligated to dephosphorylated arms of pYUB412 (XbaI-EcoRV and EcoRV-XbaI), which were the kind gifts of William R. Jacobs, Jr. (Department of Microbiology and Immunology, Albert Einstein College of Medicine, Bronx, NY). The cosmid vector pYUB412 is an *Escherichia coli-Mycobacterium* shuttle vector with the *int-attP* sequence for integration into a mycobacterial chromosome, *oriE* for replication in *E. coli*, a hygromycin resistance gene, and an ampicillin resistance gene. After in vitro packaging using Gigapack III Gold extracts (Stratagene, La Jolla, CA), recombinant cosmids were introduced into *E. coli* STBL2 [F$^-$ *mcrA* Δ(*mcrBC-hsdRMS-mrr*) *recA1 endA1 lon gyrA96 thi supE44 relA1* λ Δ(*lac-proAB*)] and stored at −80°C in 50% glycerol.

Isolation of cosmid clones carrying biosynthesis gene cluster of serotype 16 GPL and sequence analysis. Isolation of DNA from *E. coli* transductants was performed as described by Supply et al., with modifications (39). The colonies were picked, transferred to a 1.5-ml tube containing 50 μl of water, and then heated at 98°C for 5 min. After centrifugation at 14,000 rpm for 5 min, the supernatant was used as the PCR template. PCR was used to isolate cosmid clones carrying the rhamnosyltransferase (*rtfA*) gene with primers rtfA-F (5′-TTTGGAGCGACGAGTTCATC-3′) and rtfA-R (5′-GTGTAGTTGACCACG CCGAC-3′). *rtfA* encodes an enzyme responsible for the transfer of Rha to 6-d-Tal in OSE (14, 31). The insert of cosmid clone no. 253 was sequenced using a BigDye Terminator, version 3.1, cycle sequencing kit (Applied Biosystems, Foster City, CA) and an ABI Prism 310 gene analyzer (Applied Biosystems). The putative function of each open reading frame (ORF) was identified by similarity searches between the deduced amino acid sequences and known proteins using BLAST (http://www.ncbi.nlm.nih.gov/BLAST/) and FramePlot (http://www.nih.go.jp/~jun/cgi-bin/frameplot.pl) with the DNASIS computer program (Hitachi Software Engineering, Yokohama, Japan).

Transformation of *M. avium* serotype 1 strain with cosmid clone no. 253. An *M. avium* serotype 1 strain (NF113) was transformed with pYUB412-cosmid clone no. 253 by electroporation, and hygromycin-resistant colonies were iso-

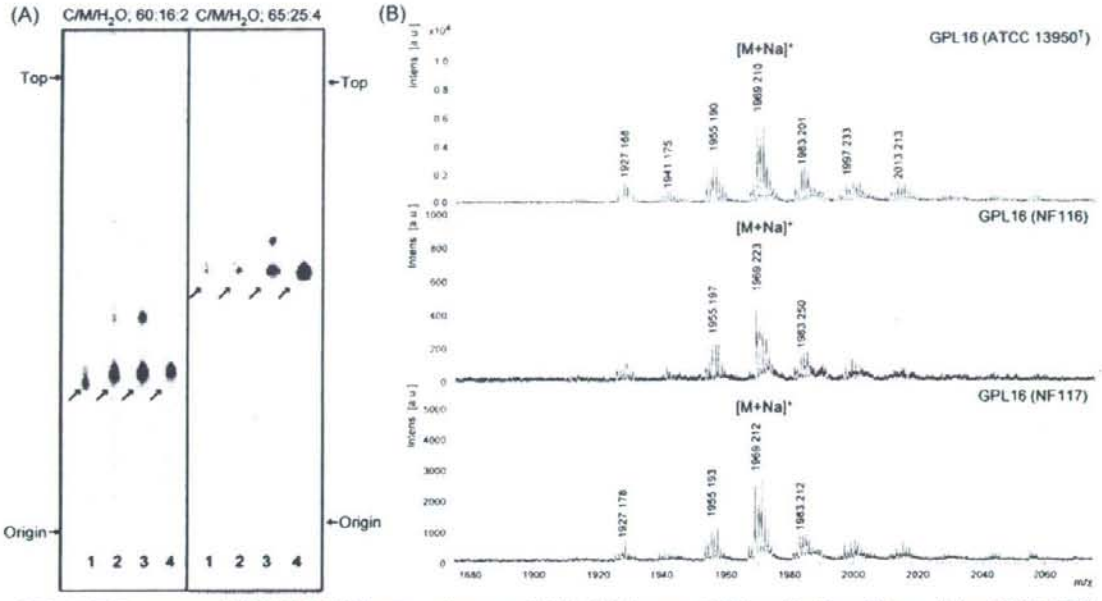

FIG. 1. TLC patterns and MALDI-TOF MS spectra of serotype 16 GPL. (A) Serotype 16 GPL purified from *M. intracellulare* ATCC 13950^T (NF 115) and the alkaline-stable lipids derived from ATCC 13950^T and two clinical isolates (NF 116 and 117) from left to right were developed on TLC plates with solvent systems of chloroform-methanol-water (65:25:4 and 60:16:2, vol/vol/vol). (B) The MALDI-TOF MS spectra were acquired using 10 mg/ml 2,5-dihydroxybenzoic acid in chloroform-methanol (1:1, vol/vol) as a matrix, and the molecularly related ions were detected as $[M+Na]^+$ in positive mode. Intens., intensity; a.u., absorbance units.

lated. Alkaline-stable lipids were prepared, and productive GPLs were examined by TLC and MALDI-TOF MS analyses.

Nucleotide sequence accession number. The nucleotide sequence reported here has been deposited in the NCBI GenBank database under accession no. AB355138.

RESULTS

Purification and molecular weight of intact GPL. Serotype 16 GPL from *M. intracellulare* ATCC 13950^T (NF 115) was detected as a spot by TLC, and the R_f values were 0.35 and 0.56 when developed with chloroform-methanol-water (60:16:2 and 65:25:4, vol/vol/vol, respectively). Two clinical isolates of *M. intracellulare*, NF 116 and 117, had serotype 16 GPLs that showed the same R_f values as the serotype 16 GPL derived from strain ATCC 13950^T. The serotype 16 GPL of *M. intracellulare* strain ATCC 13950^T was purified repeatedly by TLC and was shown as a single spot by TLC (Fig. 1A). The MALDI-TOF MS spectra of each serotype 16 GPL showed *m/z* 1969 for $[M+Na]^+$ as the main molecularly related ion in positive mode, with the homologous ions differing by 14 mass units at 1,955 and 1,983 (Fig. 1B). As a result, the main molecular weight of serotype 16 GPL was 1,946, which implied that it has a novel carbohydrate chain elongated from D-*allo*-Thr.

Carbohydrate composition of serotype 16 OSE. To determine the glycosyl compositions of serotype 16 OSE, alditol acetate derivatives of the serotype 16 GPL were analyzed by GC and GC-MS. The structurally defined serotype 4 GPL was used as a reference standard (9, 35). Comparison of the retention time and GC mass spectra (Fig. 2) with the alditol acetate derivatives of the serotype 16 GPL showed the presence of 3,4-di-*O*-Me-Rha, 4-*O*-Me-Rha, Rha, 6-d-Tal, and an unknown sugar residue (X1) in a ratio of approximately 1:1:2:1:1. The alditol acetate of X1 was eluted at a retention time of 29.3 min, greater than that of glucitol acetate on the SPB-1 column. The CI-MS spectrum of X1 was $[M+H]^+$ at *m/z* 520 as a parent ion and *m/z* 460 as a loss of 60 (acetate). The fragment ions of X1 sugar showed characteristic patterns in EI-MS. *m/z* 360 indicated the cleavage of C-3 and C-4, and *m/z* 300, 240, and 180 were fragmented with a loss of 60 (acetate). Similarly, *m/z* 374 indicated the cleavage of C-2 and C-3, and *m/z* 314 and 254 were fragmented with a loss of 60 (Fig. 3A and B). These results indicated that X1 was 3,6-dideoxy hexose (Hex). The odd molecular weight of X1, 519, and *m/z* 187, 127, and 59 implied the presence of one amido group esterified with a short-chain fatty acid, possibly. After methanolysis of serotype 16 GPL, the resultant fatty acid methyl esters were extracted carefully and analyzed by GC-MS. The EI-MS spectrum of a short-chain fatty acid methyl ester showed mass ions at *m/z* 176 ($[M]^+$), 145 ($[M-31]^+$), 117 ($[M-59]^+$), 99, 88, 85, and 59 (Fig. 3C) (33, 37). Taking the results together, X1 was structurally determined to be 3-2'-methyl-3'-hydroxy-4'-methoxy-pentanoyl-amido-3,6-dideoxy-Hex.

Glycosyl linkage and sequence of serotype 16 OSE. To determine the glycosyl linkage and sequence of the OSE, GC-MS of perdeuteromethylated alditol acetates and MALDI-TOF/TOF MS of the oligoglycosyl alditol from serotype 16 OSE

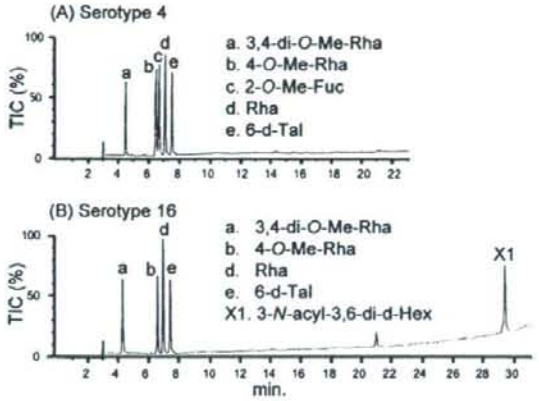

FIG. 2. Gas chromatograms of the alditol acetate derivatives from serotype 4 (A) and serotype 16 (B) GPLs. Total ion chromatograms (TIC) are shown. GC was performed on an SPB-1-fused silica column with a temperature program of 160°C for 2 min, followed by an increase of 4°C/min to 220°C, and holding at 220°C for 15 min. Comparison to the GC spectrum of serotype 4 GPL shows that serotype 16 GPL is composed of 3,4-di-*O*-Me-Rha, 4-*O*-Me-Rha, Rha, 6-d-Tal, and an unknown X1 sugar residue.

were performed. As shown in Fig. 4, the GC-MS spectra of perdeuteromethylated alditol acetates were assigned four major peaks, 1,3,4,5-tetra-*O*-deuteromethyl-2-*O*-acetyl-6-deoxy-talitol (*m/z* 109, 132, 154, 167, and 214); 2,4-di-*O*-deuteromethyl-1,3,5-tri-*O*-acetyl-rhamnitol (*m/z* 121, 134, 205, 240, and 253); 2-*O*-deuteromethyl-4-*O*-methyl-1,3,5-tri-*O*-acetyl-rhamnitol (*m/z* 121, 131, 202, and 237); and 2,4-di-*O*-deuteromethyl-1,5-di-*O*-acetyl-3-2′-methyl-3′-*O*-deuteromethyl-4′methoxy-pentanoyl-deuteromethylamido-3,6-dideoxy-hexitol (*m/z* 121, 134, and 341). These results revealed that the 6-d-Tal residue was linked at C-2; Rha and 4-*O*-Me-Rha were linked at C-1 and C-3; and the nonreducing terminus, 3-2′-methyl-3′-hydroxy-4′-methoxy-pentanoyl-amido-3,6-dideoxy-Hex, was C-1 linked. The MALDI-TOF/TOF MS spectrum of the oligoglycosyl alditol from serotype 16 OSE afforded the expected molecular ions $[M+Na]^+$ at *m/z* 931, together with the characteristic mass increments in the series of glycosyloxonium ions formed on fragmentation at *m/z* 312, 472, 618, and 764 from the terminal sugar *N*-acyl-Hex to 6-d-Tal and at *m/z* 336, 482, and 642 from 6-d-Tal to *N*-acyl-Hex (Fig. 5). Rha residues were determined to be in the L absolute configuration by comparative GC-MS analyses of trimethylsilylated (*S*)-(+)-sec-butyl glycosides and (*R*)-(−)-sec-butylglycosides (see Fig. S1 in the supplemental material). Taken together, these results established the sequence and linkage arrangement 3-2′-methyl-3′-hydroxy-4′-methoxy-pentanoyl-amido-3,6-dideoxy-Hex-(1→3)-4-*O*-Me-Rha-(1→3)-L-Rha-(1→3)-L-Rha-(1→2)-6-d-Tal, exclusively.

NMR analysis of serotype 16 OSE. The ^{1}H NMR and ^{1}H-^{1}H COSY analyses of the serotype 16 GPL revealed six distinct anomeric protons with corresponding H1-H2 cross peaks in the low field region at δ4.93, 4.92, 4.92, 4.84, 4.65 ($J_{1\text{-}2}$ = 2 to 3 Hz, indicative of α-anomers) and 4.51 (a doublet, $J_{1\text{-}2}$ = 7.7 Hz, indicative of a β-hexosyl unit). When further analyzed by

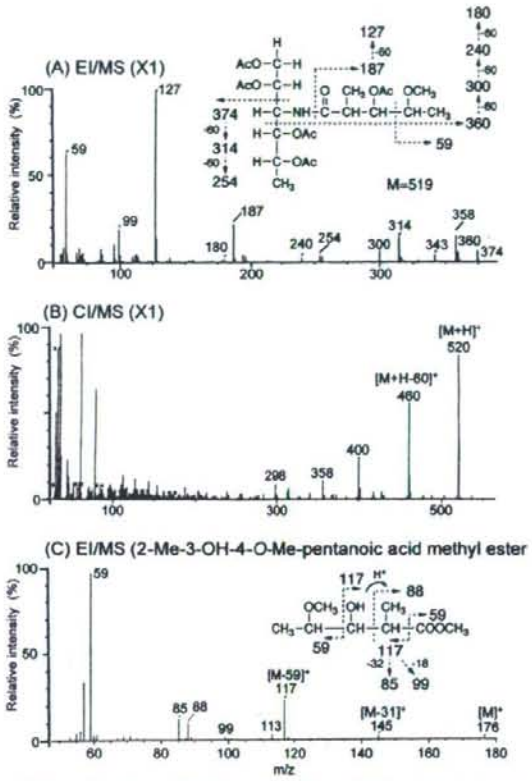

FIG. 3. EI-MS and CI-MS spectra of the alditol acetate derivative from X1 (A and B) and *N*-acylated-short-chain fatty acid methyl ester (C). The pattern of prominent fragment ions is illustrated. The CG column and condition were described in the legend for Fig. 2.

^{1}H-detected [^{1}H, ^{13}C] two-dimensional HMQC, the anomeric protons resonating at δ4.93, 4.92, 4.92, 4.84, 4.65, and 4.51 have C-1s resonating at δ101.57, 95.73, 101.40, 102.56, 100.97, and 103.36, respectively (for a summary, see Table S1 in the supplemental material). The J_{CH} values for each of these protons were calculated to be 171, 170, 171, 170, 169, and 161 Hz by measurement of the inverse-detection nondecoupled two-dimensional HMQC (Fig. 6). These results established that the terminal amido-Hex was a β configuration and the others were α-anomers.

Cloning and sequence of serotype 16 GPL biosynthesis cluster. To isolate the serotype 16 GPL biosynthesis cluster, the genomic cosmid library of *M. intracellulare* serotype 16 strain ATCC 13950^T was constructed. Primers were designed to amplify the region corresponding to the *rtfA* gene. More than 300 cosmid clones were tested using colony PCR with *rtfA* primers, and the positive clones no. 51 and 253 were isolated from the *E. coli* transductants. PCR analysis revealed that clone no. 253 contained a *drrC* gene but that clone no. 51 did not. Thus, we used clone no. 253 for subsequent sequence analysis for the *gtfB-drrC* region. The 22.9-kb region of *M. intracellulare* sero-

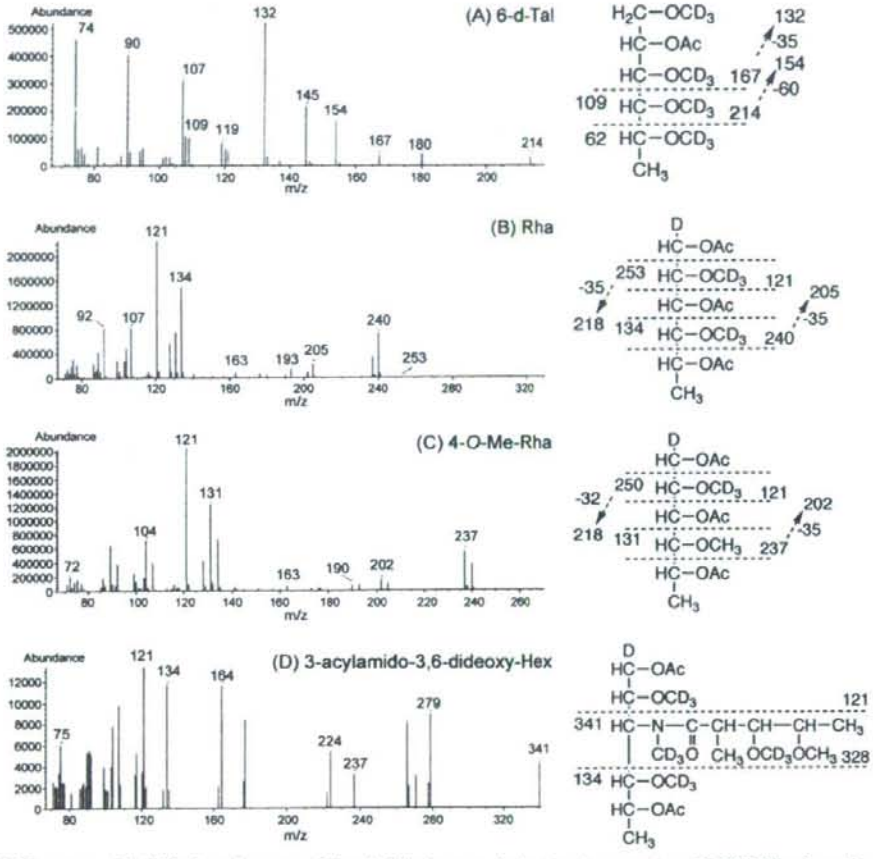

FIG. 4. GC-MS spectra of individual perdeuteromethylated alditol acetate derivatives from serotype 16 OSE. The formation of prominent fragment ions is illustrated; fragments were assigned to 1,3,4,5-tetra-*O*-deuteromethyl-2-*O*-acetyl-6-deoxy-talitol (A), 2,4-di-*O*-deuteromethyl-1,3,5-tri-*O*-acetyl-rhamnitol (B), 2-*O*-deuteromethyl-4-*O*-methyl-1,3,5-tri-*O*-acetyl-rhamnitol (C), and 2,4-di-*O*-deuteromethyl-1,5-di-*O*-acetyl-3-2′-methyl-3′-*O*-deuteromethyl-4′-methoxy-pentanoyl-deuteromethylamido-3,6-dideoxy-hexitol (D).

type 16 ATCC 13950^T was deposited in the NCBI GenBank database (accession no. AB355138). The similarity to protein sequences of each ORF is summarized in Table 1, and the genetic map for the serotype 16 GPL biosynthetic cluster was compared with those of serotype 2, 4, and 7 GPLs (Fig. 7). The *gtfB* and *drrC* genes of *M. intracellulare* serotype 16 ATCC 13950^T had 99.8% and 83.7% DNA identities with those of *M. intracellulare* serotype 7 ATCC 35847, respectively. In the DNA region between *gtfB* and *drrC* (20.8 kb), 17 ORFs were observed. Four ORFs (ORF 1, 2, 16, and 17) were homologous to those found in the same region of serotype 7-specific DNA, and the others were unique to the serotype 16 strain. No insertion of insertion elements or transposons was detected in this region. The nucleotide sequences of the ORF 1 and ORF 2 in serotype 16 strain ATCC 13950^T were homologous to those of ORF 1 and ORF 8 in serotype 7, respectively, suggesting that these two ORFs have the same function. The similarity of the deduced amino acid sequences suggested the possibility that the functions of ORF 3 and ORF 6 are to encode methyltransferase and aminotransferase, respectively. The deduced amino acid sequences of ORF 4 and ORF 5 showed significant similarities to the WxcM protein, the function of which is not clear. Interestingly, the deduced amino acid sequences of ORF 16 and ORF 17 of serotype 16 were homologous to ORF 9 of serotype 7. ORFs 1, 16, and 17 have considerable homology to glycosyltransferases. Nine ORFs, which are possibly involved in fatty acid synthesis, were detected between ORF 7 and ORF 15. It is notable that ORF 13 had a chimeric structure. The N-terminal half of ORF 13 showed similarity to phosphate butyryl/acetyl transferases, but the C-terminal half showed similarity to short-chain reductase/dehydrogenases. These results suggest that this region of DNA is responsible for the biosynthesis of the serotype 16-specific GPL.

Expression of cosmid clone no. 253 in *M. avium* serotype 1 strain. The OSE of serotype 1 GPL was composed of α-L-Rha-

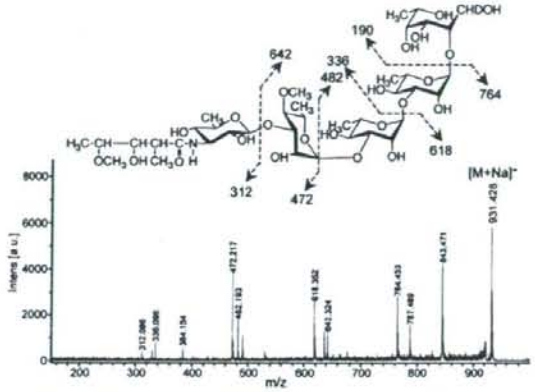

FIG. 5. MALDI-TOF/TOF MS spectrum of serotype 16 OSE. The formation of a characteristic increment in fragment ions is illustrated. The matrix was 10 mg/ml 2,5-dihydroxybenzoic acid in ethanol-water (3:7, vol/vol), and it was performed in the lift-lift mode. Intens., intensity; a.u., absorbance units.

(1→2)-6-d-L-Tal (9). The *M. avium* serotype 1 strain (NF113) was transformed with cosmid clone no. 253 containing a serotype 16-specific gene cluster and produced a new GPL with a different R_f value by TLC compared to serotype 1 GPL (Fig. 8A). The R_f value of the new GPL was identical to that of the serotype 16 GPL. The molecular weight of intact GPL, the fragment pattern of its OSE, and the GC pattern of the alditol acetate derivatives were completely equivalent to those of the serotype 16 GPL (see Fig. S2 in the supplemental material). As a result, the transformant of the serotype 1 strain expressed the cosmid clone no. 253 gene cluster and produced the serotype 16 GPL.

DISCUSSION

MAC species have serotype-specific GPLs that are characteristic components of the outer layer of the cell wall (6, 9). In addition to their serological differentiation, the chemical structures of 15 serotype-specific GPLs derived from the predominant clinical isolates have been analyzed; however, those of other GPLs remain unclear. The present study demonstrates the chemical structure of the serotype 16 GPL derived from *M. intracellulare*. We determined the glycosyl composition, linkage positions, and anomeric and ring configurations of the glycosyl residues of the serotype 16 GPL, and its OSE was defined as 3-2′-methyl-3′-hydroxy-4′-methoxy-pentanoyl-amido-3,6-dideoxy-β-Hex-(1→3)-4-*O*-methyl-α-L-Rha-(1→3)-α-L-Rha-(1→3)-α-L-Rha-(1→2)-6-d-α-L-Tal (Fig. 8B). The serotype 16 GPL should be listed as a group 2 polar GPL in the structural classification of Chatterjee and Khoo (9).

The GPLs of serotypes 7, 12, 17, and 19 have already been classified as group 2 GPLs, which are commonly composed of R→α-L-Rha-(1→3)-α-L-Rha-(1→2)-6-d-L-Tal (R, variable region), possessing a characteristic terminal sugar such as *N*-acyldeoxy-Hex. Indeed, the presence of an amido sugar has been reported in only five GPLs, serotypes 7, 12, 14, 17, and 25 (8, 9, 18). It has been determined that the OSE structure of the

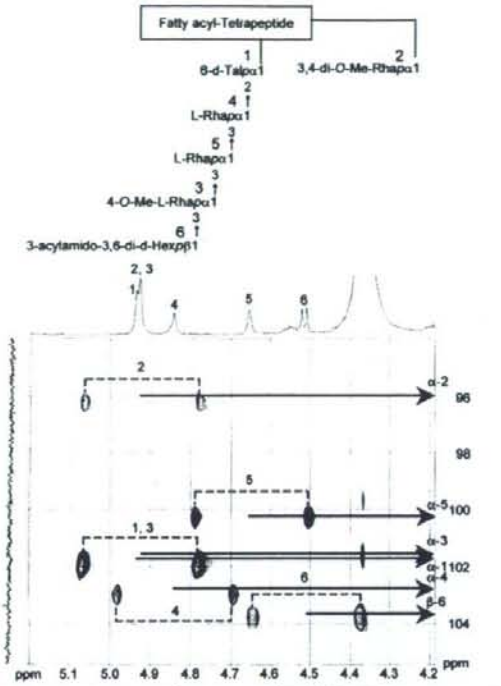

FIG. 6. Nondecoupled ^{1}H-detected [^{1}H, ^{13}C] HMQC spectrum of serotype 16 GPL. Cross-peak labels correspond to those shown on the structure.

serotype 17 GPL was 3-2′-methyl-3′-hydroxy-butanoyl-amido-3,6-dideoxy-β-D-Glc-(1→3)-4-*O*-methyl-α-L-Rha-(1→3)-α-L-Rha-(1→3)-α-L-Rha-(1→2)-6-d-L-Tal (9, 25). Based on the behavior of GPLs in TLC and the GC-MS analysis of alditol acetate derivatives, serotype 16 GPL seems to possess a unique carbohydrate epitope similar to that of serotype 17 GPL. We compared the OSE of serotype 16 GPL to that of serotype 17 GPL. The acylated amido group that was bound to the terminal sugar was different, although the linkage position was identical. Except for the terminal-acylated amido sugar, the other sugar compositions and glycosyl linkage positions were completely identical. An acylated amido group attached to the C-3 position of Hex is very unusual. To our knowledge, 3-amido-Hex is irregular in nature, although 2-amido-Hex is known to be glucosamine or galactosamine, which is frequently isolated as a component of lipopolysaccharides and glycosaminoglycans in prokaryotic and eukaryotic cells (7, 42). Further, existence of short-chain fatty acid 2-methyl-3-hydroxy-4-methoxy-pentanoic acid linked to the amido group of d-Hex is also unique. The characteristic gene cluster is thought to regulate the production of 3-acylated-amido-Hex. It is difficult to determine the species of acylated amido sugars, because no reference standard is available. The terminal sugar of the serotype 17 GPL was reviewed as a gluco-configuration, although firm evidence was not shown (9, 25). The J_{CH} and $J_{1,2}$ values for the anomeric proton in the terminal sugar were 161 and 7.7 Hz,

TABLE 1. Similarity to protein sequences of ORFs in cosmid clone no. 253 derived from *M. intracellulare* serotype 16 strain ATCC 13950^T

ORF	Predicted molecular mass (kDa)	Predicted pI	Exhibits similarity to:	E value	Amino acid identity (no. matched/total no.)	Accession no.
GtfB	45.6	6.35	Glycosyltransferase GtfB	0.0	417/418	BAF45360
Orf 1	45.2	6.10	Putative glycosyltransferase	0.0	416/417	BAF45361
Orf 2	78.9	8.51	Putative acyltransferase	0.0	557/728	BAF45368
Orf 3	31.0	5.88	Putative methyltransferase	2e-89	382/421	NP_218045
Orf 4	15.7	4.94	Conserved hypothetical protein	1e-39	73/129	BAD50406
Orf 5	16.0	4.69	Conserved hypothetical protein	5e-40	75/135	EAX55190
Orf 6	41.1	5.88	Aminotransferase/DegT_DnrJ_EryC1	6e-119	208/357	ABD68440
Orf 7	40.6	9.65	Conserved hypothetical protein	2e-89	178/304	AAS03547
Orf 8	36.7	5.32	Conserved hypothetical protein	2e-52	116/298	CAE06954
Orf 9	22.3	9.79	Putative *N*-acetyltransferase	4e-14	58/166	EAU11841
Orf 10	25.3	7.82	Short-chain dehydrogenase/reductase	7e-47	101/233	EAO61220
Orf 11	23.8	6.05	Putative hydrolase	4e-24	64/196	ABG85599
Orf 12	37.2	6.50	Ketoacyl-acyl carrier protein synthase III	3e-55	126/331	EAX48715
Orf 13	42.5	7.72	Short-chain dehydrogenase/reductase	2e-42	97/248	ZP_01289005
Orf 14	65.8	4.70	Predicted enzyme involved in methoxymalonyl-acyl carrier protein biosynthesis	6e-85	201/575	ABB73590
Orf 15	50.0	6.23	Acyl coenzyme A synthetases	2e-128	233/445	EAT27362
Orf 16	39.1	8.00	Putative glycosyltransferase	2e-106	196/318	NP_855197
Orf 17	37.7	9.46	Putative glycosyltransferase	8e-160	278/323	BAF45369
DrrC	28.6	11.47	Daunorubicin resistance protein C	6e-132	233/261	BAF45370

respectively (Fig. 6; Table S1 in the supplemental material). These results demonstrated unequivocally that the terminal amido-Hex was β configuration and H-2 was in the axial position. The terminal amido-Hex is considered to be derived from glucose or galactose, not Rha.

Next, we explored the genetic mechanism of GPL biosynthesis, because the elongation of carbohydrate chains in serotype-specific GPLs is poorly understood. The *ser2* gene cluster of the *M. avium* serotype 2 strain (31) and a 27.5-kb DNA fragment of the *M. avium* serotype 4 strain (28) were identified to be responsible for the biosynthesis of each OSE in GPLs. Recently, enzymatic characterizations of glycosyltransferase and methyltransferase of nonpolar GPLs have been reported for *Mycobacterium smegmatis* (36, 38). In the serotype-specific polar GPL biosynthesis of MAC, only the *rtfA* gene was functionally clarified to encode the transfer of L-Rha to 6-d-Tal, but which gene cluster transfers the sugars next to L-Rha elongated from 6-d-Tal is unclear.

In this study, we cloned the biosynthetic cluster of the serotype 16 GPL and analyzed its sequence. Seventeen ORFs were detected in the serotype 16 strain, and the sequence homology was analyzed. The transformant of the *M. avium* serotype 1

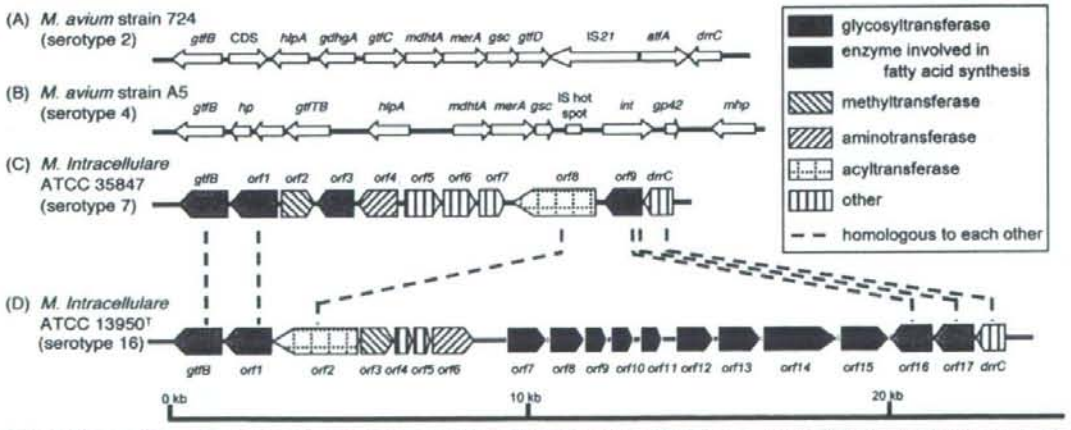

FIG. 7. Comparison and overview of genetic maps of GPL biosynthetic cluster. The *M. avium* strain 724 annotated sequence obtained from GenBank (accession no. AF125999) (A); the *M. avium* strain A5 annotated sequence obtained from GenBank (accession no. AY130970) (B); the *M. intracellulare* ATCC 35847 sequenced in our previous study (GenBank accession no. AB274811) (C); the *M. intracellulare* ATCC 13950^T sequenced in this study (GenBank accession no. AB355138) (D). The orientation of each gene is shown by the direction of the arrow. In panels A and B, putative ORFs not showing homology to known proteins sequences are not depicted. The sequences extending upstream in panels A and B and downstream in panel B are not included in the figure.

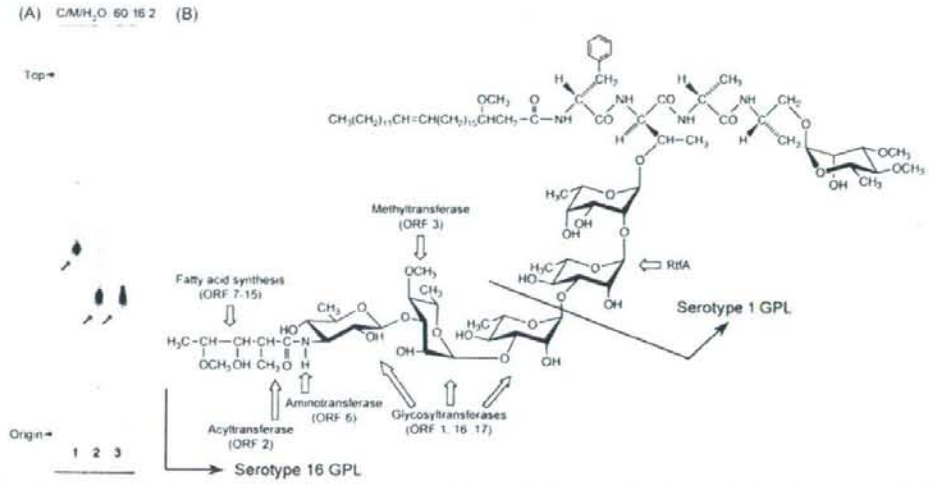

FIG. 8. TLC pattern of *M. avium* serotype 1 and its transformant with cosmid clone no. 253 and proposed complete structure of the serotype 16 GPL. (A) The alkaline-stable lipids derived from *M. avium* serotype 1 (lane 1), its transformant (lane 2), and purified serotype 16 GPL (lane 3) were developed with the solvent system of chloroform-methanol-water (60:16:2, vol/vol/vol). (B) Predicted biosynthesis gene clusters are indicated by arrows.

strain carrying cosmid clone no. 253 produced serotype 16 GPL. These results strongly implied that this *gtfB-drrC* region is responsible for the biosynthesis of the serotype 16-specific GPL. From the structural analysis of the serotype 16 GPL and the sequence of cosmid clone no. 253, it is possible to predict the relationship between the biosynthesis of serotype 16 GPL and the function of each ORF.

The genetic map of the serotype 16 GPL biosynthetic cluster was compared to those of serotype 2 GPL from *M. avium* strain 724, serotype 4 GPL from *M. avium* strain A5, and serotype 7 GPL from *M. intracellulare* strain ATCC 35847^T (12, 18, 28). Significant differences were found in the neighborhood of the conserved region. The genetic organization of the serotype 16 GPL gene cluster was distinct from that of serotype 7, except for some of the ORFs, and the ORFs in this region of serotype 2 and serotype 4 were completely different from ORFs 1 to 17 in serotype 16 (Fig. 7).

In addition to *M. intracellulare* serotype 7 (18) and serotype 16 strains, we have analyzed similar gene clusters of *M. intracellulare* serotype 12 and 17 strains. The sequence homology of the regions of ORF 1 and ORF 17 was highly conserved between only *M. intracellulare* serotype 16 and 17 strains (unpublished data). ORFs 1, 16, and 17 may lead to transfer of the two additional molecules of L-Rha and terminal amido-Hex. ORF 2 was assigned to acyltransferase and may be responsible for biosynthesis of the 3-2′-methyl-3′-hydroxy-4′-methoxy-pentanoyl-amido group in the terminal Hex. ORF 3 is probably responsible for the transfer of the *O*-methyl group at the C-4 position in the third L-Rha from 6-d-Tal. ORF 6 is homologous to aminotransferase and possibly associated with the biosynthesis of an amido group in the terminal Hex. The deduced amino acid sequences of ORF 6 in serotype 16 and ORF 4 in serotype 7 have homologies to DegT_DnrJ_EryC1 aminotransferases. However, these two ORFs are dissimilar to each other. Serotype 16 and 7 GPLs have an amido group at the terminal Hex, although the attachment position is different. The serotype 7 GPL has an amido group at the C-4 position in the terminal Hex, but the serotype 16 GPL has it at the C-3 position. Nine ORFs between ORF 7 and ORF 15 are possibly involved in fatty acid synthesis of the acyl chain moiety linked by an amido bond of the terminal Hex. Taken together, this gene cluster may participate in the biosynthetic pathway of the serotype 16-specific GPL, although further study is needed to clarify the function of each ORF.

Recent studies suggest that GPLs play an important role in the phenotype and pathogenicity of MAC. The colony morphology is considered to be influenced by cell wall GPL. MAC colony phenotypes spontaneously occur from smooth to rough type, and this is due to a mutation lacking GPL (3, 13, 22). The deletion of genomic regions encoding GPL biosynthesis may result in the loss of GPL. Danelishvili et al. demonstrated that the uptake by and growth in macrophages of a MAC mutant with the gene belonging to the GPL synthesis pathway inactivated by transposon insertion were decreased (11). Bhatnagar and Schorey have reported that macrophages infected with MAC release exosomes containing GPLs that result in the transfer of the GPLs to uninfected macrophages and induce a proinflammatory response (4). These findings imply that GPL participates in the pathogenicity of MAC. By contrast, our previous studies have demonstrated that anti-GPL antibodies are detected in the sera of most immunocompetent patients with MAC pulmonary disease and that the detection of anti-GPL antibody is useful for the serodiagnosis of MAC disease (15, 26, 27).

To understand the role of GPLs in MAC and its hosts, it is necessary to define the chemical structure and biosynthesis pathways of GPLs. Elucidation of the structure-function relationship of GPL may open a new avenue for controlling MAC disease.

ACKNOWLEDGMENTS

This work was supported by grants from the Ministry of Education, Culture, Sports, Science, and Technology of Japan, the Japan Health Sciences Foundation, and the Ministry of Health, Labor, and Welfare of Japan (Research on Emerging and Reemerging Infectious Diseases).

We are grateful to Sumihiro Hase (Department of Chemistry, Graduate School of Science, Osaka University, Osaka, Japan) and Hiromi Murakami (Osaka Municipal Technical Research Institute, Osaka, Japan) for helpful discussion.

REFERENCES

1. **Baess, I.** 1983. Deoxyribonucleic acid relationships between different serovars of *Mycobacterium avium*, *Mycobacterium intracellulare* and *Mycobacterium scrofulaceum*. Acta Pathol. Microbiol. Immunol. Scand. **91:**201–203.
2. **Barrow, W. W., T. L. Davis, E. L. Wright, V. Labrousse, M. Bachelet, and N. Rastogi.** 1995. Immunomodulatory spectrum of lipids associated with *Mycobacterium avium* serovar 8. Infect. Immun. **63:**126–133.
3. **Belisle, J. T., K. Klaczkiewicz, P. J. Brennan, W. R. Jacobs, Jr., and J. M. Inamine.** 1993. Rough morphological variants of *Mycobacterium avium*. Characterization of genomic deletions resulting in the loss of glycopeptidolipid expression. J. Biol. Chem. **268:**10517–10523.
4. **Bhatnagar, S., and J. S. Schorey.** 2007. Exosomes released from infected macrophages contain *Mycobacterium avium* glycopeptidolipids and are proinflammatory. J. Biol. Chem. **282:**25779–25789.
5. **Bhatt, A., N. Fujiwara, K. Bhatt, S. S. Gurcha, L. Kremer, B. Chen, J. Chan, S. A. Porcelli, K. Kobayashi, G. S. Besra, and W. R. Jacobs, Jr.** 2007. Deletion of *kasB* in *Mycobacterium tuberculosis* causes loss of acid-fastness and subclinical latent tuberculosis in immunocompetent mice. Proc. Natl. Acad. Sci. USA **104:**5157–5162.
6. **Brennan, P. J., and H. Nikaido.** 1995. The envelope of mycobacteria. Annu. Rev. Biochem. **64:**29–63.
7. **Campo, G. M., S. Campo, A. M. Ferlazzo, R. Vinci, and A. Calatroni.** 2001. Improved high-performance liquid chromatographic method to estimate aminosugars and its application to glycosaminoglycan determination in plasma and serum. J. Chromatogr. B **765:**151–160.
8. **Chatterjee, D., G. O. Aspinall, and P. J. Brennan.** 1987. The presence of novel glucuronic acid-containing, type-specific glycolipid antigens within *Mycobacterium* spp. Revision of earlier structures. J. Biol. Chem. **262:**3528–3533.
9. **Chatterjee, D., and K. H. Khoo.** 2001. The surface glycopeptidolipids of mycobacteria: structures and biological properties. Cell. Mol. Life Sci. **58:** 2018–2042.
10. **Daffe, M., and P. Draper.** 1998. The envelope layers of mycobacteria with reference to their pathogenicity. Adv. Microb. Physiol. **39:**131–203.
11. **Danelishvili, L., M. Wu, B. Stang, M. Harriff, S. Cirillo, J. Cirillo, R. Bildfell, B. Arbogast, and L. E. Bermudez.** 2007. Identification of *Mycobacterium avium* pathogenicity island important for macrophage and amoeba infection. Proc. Natl. Acad. Sci. USA **104:**11038–11043.
12. **Eckstein, T. M., J. T. Belisle, and J. M. Inamine.** 2003. Proposed pathway for the biosynthesis of serovar-specific glycopeptidolipids in *Mycobacterium avium* serovar 2. Microbiology **149:**2797–2807.
13. **Eckstein, T. M., J. M. Inamine, M. L. Lambert, and J. T. Belisle.** 2000. A genetic mechanism for deletion of the *ser2* gene cluster and formation of rough morphological variants of *Mycobacterium avium*. J. Bacteriol. **182:** 6177–6182.
14. **Eckstein, T. M., F. S. Silbaq, D. Chatterjee, N. J. Kelly, P. J. Brennan, and J. T. Belisle.** 1998. Identification and recombinant expression of a *Mycobacterium avium* rhamnosyltransferase gene (*rtfA*) involved in glycopeptidolipid biosynthesis. J. Bacteriol. **180:**5567–5573.
15. **Enomoto, K., S. Oka, N. Fujiwara, T. Okamoto, Y. Okuda, R. Maekura, T. Kuroki, and I. Yano.** 1998. Rapid serodiagnosis of *Mycobacterium avium-intracellulare* complex infection by ELISA with cord factor (trehalose 6, 6′-dimycolate), and serotyping using the glycopeptidolipid antigen. Microbiol. Immunol. **42:**689–696.
16. **Falkinham, J. O., III.** 1996. Epidemiology of infection by nontuberculous mycobacteria. Clin. Microbiol. Rev. **9:**177–215.
17. **Field, S. K., D. Fisher, and R. L. Cowie.** 2004. *Mycobacterium avium* complex pulmonary disease in patients without HIV infection. Chest **126:**566–581.
18. **Fujiwara, N., N. Nakata, S. Maeda, T. Naka, M. Doe, I. Yano, and K. Kobayashi.** 2007. Structural characterization of a specific glycopeptidolipid containing a novel *N*-acyl-deoxy sugar from *Mycobacterium intracellulare* serotype 7 and genetic analysis of its glycosylation pathway. J. Bacteriol. **189:**1099–1108.
19. **Gerwig, G. J., J. P. Kamerling, and J. F. G. Vliegenthart.** 1978. Determination of the D and L configuration of neutral monosaccharides by high-resolution capillary G.L.C. Carbohydr. Res. **62:**349–357.
20. **Hakomori, S.** 1964. A rapid permethylation of glycolipid, and polysaccharide catalyzed by methylsulfinyl carbanion in dimethyl sulfoxide. J. Biochem. (Tokyo) **55:**205–208.
21. **Heidelberg, T., and O. R. Martin.** 2004. Synthesis of the glycopeptidolipid of *Mycobacterium avium* serovar 4: first example of a fully synthetic C-mycoside GPL. J. Org. Chem. **69:**2290–2301.
22. **Howard, S. T., E. Rhoades, J. Recht, X. Pang, A. Alsup, R. Kolter, C. R. Lyons, and T. F. Byrd.** 2006. Spontaneous reversion of *Mycobacterium abscessus* from a smooth to a rough morphotype is associated with reduced expression of glycopeptidolipid and reacquisition of an invasive phenotype. Microbiology **152:**1581–1590.
23. **Kaufmann, S. H.** 2001. How can immunology contribute to the control of tuberculosis? Nat. Rev. Immunol. **1:**20–30.
24. **Khoo, K. H., D. Chatterjee, A. Dell, H. R. Morris, P. J. Brennan, and P. Draper.** 1996. Novel *O*-methylated terminal glucuronic acid characterizes the polar glycopeptidolipids of *Mycobacterium habana* strain TMC 5135. J. Biol. Chem. **271:**12333–12342.
25. **Khoo, K. H., E. Jarboe, A. Barker, J. Torrelles, C. W. Kuo, and D. Chatterjee.** 1999. Altered expression profile of the surface glycopeptidolipids in drug-resistant clinical isolates of *Mycobacterium avium* complex. J. Biol. Chem. **274:**9778–9785.
26. **Kitada, S., R. Maekura, N. Toyoshima, N. Fujiwara, I. Yano, T. Ogura, M. Ito, and K. Kobayashi.** 2002. Serodiagnosis of pulmonary disease due to *Mycobacterium avium* complex with an enzyme immunoassay that uses a mixture of glycopeptidolipid antigens. Clin. Infect. Dis. **35:**1328–1335.
27. **Kitada, S., Y. Nishiuchi, T. Hiraga, N. Naka, H. Hashimoto, K. Yoshimura, K. Miki, M. Miki, M. Motone, T. Fujikawa, K. Kobayashi, I. Yano, and R. Maekura.** 2007. Serological test and chest computed tomography findings in patients with *Mycobacterium avium* complex lung disease. Eur. Respir. J. **29:**1217–1223.
28. **Krzywinska, E., and J. S. Schorey.** 2003. Characterization of genetic differences between *Mycobacterium avium* subsp. avium strains of diverse virulence with a focus on the glycopeptidolipid biosynthesis cluster. Vet. Microbiol. **91:**249–264.
29. **Maekura, R., Y. Okuda, A. Hirotani, S. Kitada, T. Hiraga, K. Yoshimura, I. Yano, K. Kobayashi, and M. Ito.** 2005. Clinical and prognostic importance of serotyping *Mycobacterium avium-Mycobacterium intracellulare* complex isolates in human immunodeficiency virus-negative patients. J. Clin. Microbiol. **43:**3150–3158.
30. **Marras, T. K., and C. L. Daley.** 2002. Epidemiology of human pulmonary infection with nontuberculous mycobacteria. Clin. Chest Med. **23:**553–567.
31. **Maslow, J. N., V. R. Irani, S. H. Lee, T. M. Eckstein, J. M. Inamine, and J. T. Belisle.** 2003. Biosynthetic specificity of the rhamnosyltransferase gene of *Mycobacterium avium* serovar 2 as determined by allelic exchange mutagenesis. Microbiology **149:**3193–3202.
32. **McClatchy, J. K.** 1981. The seroagglutination test in the study of nontuberculous mycobacteria. Rev. Infect. Dis. **3:**867–870.
33. **McCloskey, J. A.** 1969. Mass spectrometry, p. 402. *In* J. M. Lowenstein (ed.), Methods in enzymology: lipid, vol. 14. Academic Press, New York, NY.
34. **McNeil, M., H. Gaylord, and P. J. Brennan.** 1988. *N*-formylkansosaminyl-(1-3)-2-*O*-methyl-D-rhamnopyranose: the type-specific determinant of serovariant 14 of the *Mycobacterium avium* complex. Carbohydr. Res. **177:**185–198.
35. **McNeil, M., A. Y. Tsang, and P. J. Brennan.** 1987. Structure and antigenicity of the specific oligosaccharide hapten from the glycopeptidolipid antigen of *Mycobacterium avium* serotype 4, the dominant *Mycobacterium* isolated from patients with acquired immune deficiency syndrome. J. Biol. Chem. **262:** 2630–2635.
36. **Miyamoto, Y., T. Mukai, N. Nakata, Y. Maeda, M. Kai, T. Naka, I. Yano, and M. Makino.** 2006. Identification and characterization of the genes involved in glycosylation pathways of mycobacterial glycopeptidolipid biosynthesis. J. Bacteriol. **188:**86–95.
37. **Odham, G., and E. Stenhagen.** 1972. Fatty acids, p. 211–228. *In* G. R. Waller (ed.), Biochemical application of mass spectrometry. Wiley-Interscience, New York, NY.
38. **Patterson, J. H., M. J. McConville, R. E. Haites, R. L. Coppel, and H. Billman-Jacobe.** 2000. Identification of a methyltransferase from *Mycobacterium smegmatis* involved in glycopeptidolipid synthesis. J. Biol. Chem. **275:**24900–24906.
39. **Supply, P., E. Mazars, S. Lesjean, V. Vincent, B. Gicquel, and C. Locht.** 2000. Variable human minisatellite-like regions in the *Mycobacterium tuberculosis* genome. Mol. Microbiol. **36:**762–771.
40. **Tsang, A. Y., J. C. Denner, P. J. Brennan, and J. K. McClatchy.** 1992. Clinical and epidemiological importance of typing of *Mycobacterium avium* complex isolates. J. Clin. Microbiol. **30:**479–484.
41. **Wayne, L. G., and H. A. Sramek.** 1992. Agents of newly recognized or infrequently encountered mycobacterial diseases. Clin. Microbiol. Rev. **5:**1–25.
42. **Woods, A., and J. R. Couchman.** 2001. Proteoglycan isolation and analysis, p. 10.7.1–10.7.19. *In* J. S. Bonifacino, M. Dasso, J. B. Harford, J. Lippincott-Schwartz, and K. M. Yamada (ed.), Current protocols in cell biology. Wiley Interscience, Hoboken, NJ.

Potent Antimycobacterial Activity of Mouse Secretory Leukocyte Protease Inhibitor[1]

Junichi Nishimura,*§ Hiroyuki Saiga,*‡ Shintaro Sato,¶ Megumi Okuyama,‖ Hisako Kayama,*‡ Hirotaka Kuwata,* Sohkichi Matsumoto,‖ Toshirou Nishida,§ Yoshiki Sawa,§ Shizuo Akira,¶ Yasunobu Yoshikai,† Masahiro Yamamoto,‡ and Kiyoshi Takeda[2]*‡

Secretory leukocyte protease inhibitor (SLPI) has multiple functions, including inhibition of protease activity, microbial growth, and inflammatory responses. In this study, we demonstrate that mouse SLPI is critically involved in innate host defense against pulmonary mycobacterial infection. During the early phase of respiratory infection with *Mycobacterium bovis* bacillus Calmette-Guérin, SLPI was produced by bronchial and alveolar epithelial cells, as well as alveolar macrophages, and secreted into the alveolar space. Recombinant mouse SLPI effectively inhibited in vitro growth of bacillus Calmette-Guérin and *Mycobacterium tuberculosis* through disruption of the mycobacterial cell wall structure. Each of the two whey acidic protein domains in SLPI was sufficient for inhibiting mycobacterial growth. Cationic residues within the whey acidic protein domains of SLPI were essential for disruption of mycobacterial cell walls. Mice lacking SLPI were highly susceptible to pulmonary infection with *M. tuberculosis*. Thus, mouse SLPI is an essential component of innate host defense against mycobacteria at the respiratory mucosal surface. *The Journal of Immunology*, 2008, 180: 4032–4039.

Mycobacterium tuberculosis is a top killer among bacterial pathogens and is responsible for 2 million deaths annually. The emergence of AIDS and development of multidrug-resistant *M. tuberculosis* have increased the incidence of tuberculosis, and it has now become a serious problem. Therefore, the host defense mechanisms against *M. tuberculosis* have been intensively investigated and important roles of T cell-mediated adaptive immunity are now well established (1, 2). In addition, functional characterization of TLRs has recently indicated the importance of innate immunity in infection with *M. tuberculosis* (3, 4). Macrophages and dendritic cells are the major effectors of TLR-mediated antimycobacterial immune responses, because they produce a variety of proinflammatory cytokines and have the capacity of phagocytosis. However, during *M. tuberculosis* infection, epithelial cells in the respiratory tract as well as alveolar macrophages are the first targets for invasion by *M. tuberculosis*. Therefore, these epithelial cells are expected to play roles in preventing mycobacterial infection by establishing physical barriers and producing proinflammatory and antimicrobial mediators (5).

Secretory leukocyte protease inhibitor (SLPI)[3] is a 12-kDa secreted protein composed of two cysteine-rich whey acidic protein (WAP) domains (also called WAP four-disulfide core (WFDC) domains) (6–8). It was originally identified in seminal fluid and is produced by secretory cells in the genital, respiratory, and lacrimal glands as well as dermal keratinocytes (9–13). SLPI is a potent inhibitor of serine proteases, such as neutrophil elastase and cathepsin G, and has therefore been proposed to protect tissues from protease-mediated damage at sites of inflammation (14, 15). Indeed, SLPI was subsequently shown to mediate wound healing (16, 17). Further studies have revealed that SLPI has additional functions. For example, it possesses an antimicrobial activities against Gram-negative and Gram-positive bacteria, fungi, and viruses, including HIV (18–20). In addition to SLPI, several other serine protease inhibitors containing a single WAP domain, such as Eppin, Elafin, SWAM1, and SWAM2, also possess antimicrobial activities against Gram-negative and Gram-positive bacteria (8, 21, 22). Thus, serine protease inhibitors possessing WAP domains exhibit antimicrobial activities. However, the precise mechanisms by which these serine protease inhibitors exert their antimicrobial activities remain elusive. More recently, SLPI was found to mediate anti-inflammatory responses. Briefly, SLPI is induced in monocytes and macrophages in response to inflammatory stimuli mediated by TLRs (23) and subsequently suppresses TLR-dependent production of inflammatory mediators in macrophages by modulating NF-κB activity (23–25). Consistent with these findings, SLPI-deficient mice are highly sensitive to TLR4 ligand (LPS)-induced endotoxin shock with increased production of IL-6 (26). Thus, SLPI has diverse functions and its precise roles need to be investigated more carefully.

*Deparment of Molecular Genetics and †Division of Host Defense, Research Center for Prevention of Infectious Diseases, Medical Institute of Bioregulation, Kyushu University, Fukuoka; ‡Laboratory of Immune Regulation, Department of Microbiology and Immunology, §Department of Surgery, Graduate School of Medicine, and ¶Department of Host Defense, Research Institute for Microbial Diseases, Osaka University; and ‖Department of Host Defense, Osaka City University Graduate School of Medicine, Osaka, Japan

Received for publication April 3, 2007. Accepted for publication January 9, 2008.

The costs of publication of this article were defrayed in part by the payment of page charges. This article must therefore be hereby marked *advertisement* in accordance with 18 U.S.C. Section 1734 solely to indicate this fact.

[1] This work was supported by a Grant-in-Aid from the Ministry of Education, Culture, Sports, Science and Technology and the Ministry of Health, Labor and Welfare, as well as the Tokyo Biochemical Research Foundation, the Cell Science Research Foundation, the Yakult Bio-Science Foundation, the Osaka Foundation for Promotion of Clinical Immunology, the Sumitomo Foundation, and the Sankyo Foundation of Life Science.

[2] Address correspondence and reprint requests to Dr. Kiyoshi Takeda, Laboratory of Immune Regulation, Department of Microbiology and Immunology, Graduate School of Medicine, Osaka University, Suita, Osaka, 565-0871, Japan. E-mail address: ktakeda@ongene.med.osaka-u.ac.jp

[3] Abbreviations used in this paper: SLPI, secretory leukocyte protease inhibitor; WAP, whey acidic protein; WFDC, WAP four-disulfide core; qPCR, quantitative PCR; BALF, bronchoalveolar lavage fluid; BCG, bacillus Calmette-Guérin; FLUOS, 5-(6-)carboxyfluorescein-*N*-hydroxysuccinimide ester; NPN, 1-*N*-phenylnapthylamine; AEC, alveolar epithelial cell.

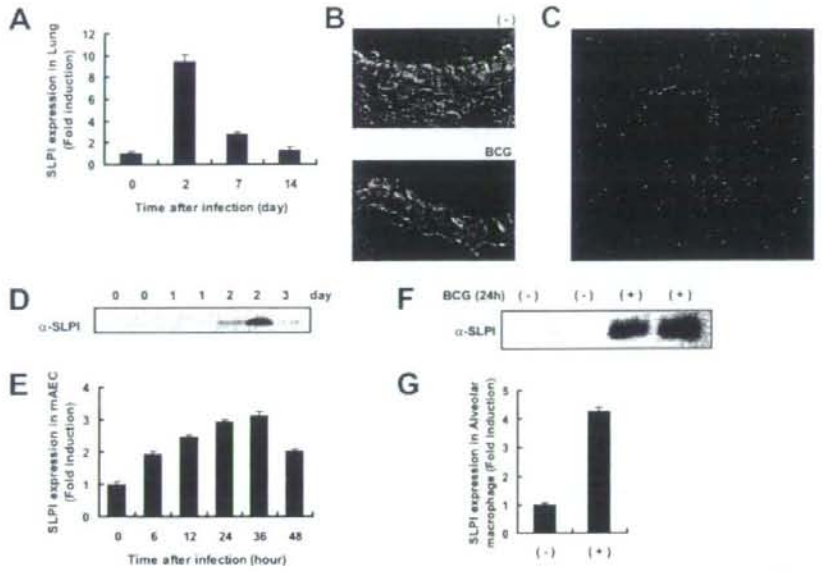

FIGURE 1. Expression of SLPI during mycobacterium infection. *A*, Wild-type mice were intratracheally infected with BCG (4×10^5 CFU). At the indicated periods, total RNA was extracted from the lungs. SLPI mRNA expression was analyzed by quantitative real-time RT-PCR. Data are shown as the relative mRNA levels normalized by the corresponding 18S rRNA level. *B* and *C*, At 2 days after intratracheal infection with BCG, lung tissue sections were stained with an anti-SLPI Ab (red) and 4′,6-diamidino-2-phenylindole (blue) and visualized by fluorescence microscopy. *D*, BALF was collected at the indicated periods after BCG infection. Mouse SLPI protein expression was analyzed by Western blotting with an anti-SLPI Ab. Data obtained from two independent mice (0, 1, and 2 days) are indicated. *E*, AEC were incubated with the same number of BCG for the indicated periods. SLPI mRNA expression was analyzed by quantitative real-time RT-PCR. Data are shown as the relative mRNA levels normalized by the corresponding 18S rRNA level. *F*, AEC were incubated with the same number of BCG. Culture supernatants were collected before (−) and after 24 h of infection (+) and subjected to Western blot analysis using an anti-SLPI Ab. Data obtained from two independent cell clones are shown. *G*, Alveolar macrophages were collected from uninfected wild-type mice, cultured with or without BCG for 48 h, and then analyzed for their SLPI mRNA expression by quantitative real-time RT-PCR. The results are presented as the mean ± SD.

In this study, we investigated the roles of murine SLPI in the context of host defenses against mycobacteria, since SLPI expression is greatly induced in macrophages and the lungs during mycobacterial infection (27). Recombinant SLPI inhibited mycobacterial growth at a lower concentration than that required to inhibit bacterial growth. Inhibition of mycobacterial growth was mediated by increased permeability of the mycobacterial membrane. Mutation of cationic residues in the WAP domains of SLPI resulted in loss of its antimycobacterial activity. Furthermore, SLPI-deficient mice were highly susceptible to pulmonary infection with *M. tuberculosis*. These findings demonstrate that SLPI is a potent antimycobacterial molecule.

Materials and Methods

Cells and bacteria

M. tuberculosis strains H37Ra (ATCC 25177; American Type Culture Collection) and *M. tuberculosis* strains H37Rv (28) were grown in Middlebrook 7H9-ADC medium for 2 wk and stored at −80°C until use. *Mycobacterium bovis* bacillus Calmette-Guérin (BCG; Tokyo strain) was purchased from Kyowa Pharmaceuticals. *Salmonella enterica* serovar *typhimurium* were provided by the Research Institute for Microbial Diseases (Osaka University). For each experiment, the dose was confirmed by plating an aliquot of the injected bacterial suspension. Isolation and immortalization of type II alveolar epithelial cells from the lungs of transgenic H-2K^b-tsA58 mice were performed as previously described (29), with some modifications.

Immunohistochemistry

Lungs were washed with PBS and frozen in Tissue-Tex OCT compound (Sakura, Tokyo, Japan). Cryostat sections (5-μm thick) were fixed with cold acetone for 10 min, dried, rehydrated with PBS, and blocked with PBS containing 20 mM HEPES, 10% FBS, and 1 μg of Fc-blocking mAb (2.4G2; BD Pharmingen). Next, the sections were sequentially incubated with a biotinylated anti-mouse SLPI Ab (R&D Systems) and Alexa Fluor 594-conjugated streptavidin (Molecular Probes). The nuclei were stained with 4′,6-diamidino-2-phenylindole (Molecular Probes). After washing with PBS, the sections were analyzed by confocal microscopy (Zeiss).

Western blot analysis

Samples were boiled for 5 min in reducing SDS-PAGE sample buffer and then subjected to SDS-PAGE. The separated proteins were transferred to a 0.45-μm pore polyvinylidene fluoride membrane (Millipore). After blocking with 5% milk, the membrane was incubated with the above-described biotinylated anti-mouse SLPI Ab (0.2 μg/ml) and a streptavidin-HRP complex (1/10,000 dilution; R&D Systems). The bound Abs were detected by the Super Signal reagent (Pierce).

Quantitative real-time RT-PCR

After isolation of total RNA with the TRIzol reagent (Invitrogen Life Technologies), 4 μg of the RNA was treated with RQ1DNase (Promega) and then reverse-transcribed using Moloney murine leukemia virus reverse transcriptase (Promega) and Random Primers (Toyobo). Gene expression was quantified with an Applied Biosystems PRISM 7000 sequence detection system using TaqMan Universal PCR Master Mix (Applied Biosystems). To determine the relative expression level of each sample, the corresponding 18S rRNA expression level was measured as an internal control. The primer and probe sequences for SLPI were follows: quantitative PCR (qPCR) primer (forward), 5′-d(GCTGTGAGGGTATATGTG GGAAA)-3′; qPCR primer (reverse), 5′-d(CGCCAATGTCAGGGAT CAG)-3′; and qPCR probe, 5′-FAMd(TCTGCCTGCCCCCGATGTG AG)BHQ-3′.

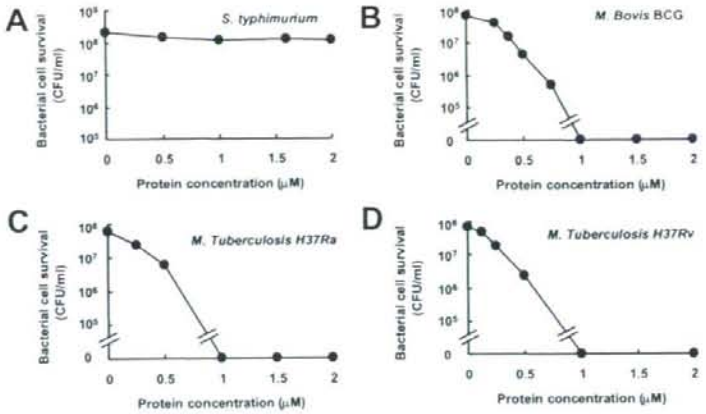

FIGURE 2. Mouse recombinant SLPI inhibits in vitro BCG and *M. tuberculosis* growth. *A*, *S. typhimurium* (5×10^7 CFU/ml) were incubated with SLPI for 2 h and plated on LB agar plates. *B–D*, BCG (*B*), *M. tuberculosis* H37Ra (*C*), or *M. tuberculosis* H37Rv (*D*; 5×10^7 CFU/ml) were incubated with increasing concentrations of recombinant mouse SLPI for 24 h and then plated on 7H10 agar plates.

Bronchoalveolar lavage fluid (BALF)

Mice were intratracheally administered 4×10^5 CFU of BCG suspended in 30 μl of PBS. BALF was collected at the indicated periods. To obtain alveolar macrophages, BALF was centrifuged at 2000 × g for 2 min and the pellet was resuspended in RPMI 1640 containing 4% FBS. The cell count of alveolar macrophages was $\sim 1 \times 10^5$ cells/mouse. To eliminate contamination by bacteria, alveolar macrophages were cultured with 50 U/ml penicillin and 50 μg/ml streptomycin for 16 h, washed five times, and infected with 5×10^7 CFU/well of BCG without penicillin and streptomycin.

Preparation of recombinant SLPI protein and variants

PCR-amplified mouse SLPI cDNA fragments were inserted into pGEX-6P-1 (Amersham Biosciences). pGEX-6P-1 containing mouse SLPI cDNA was transformed into *Escherichia coli* Rosetta-gami B (DE 3). Expression of GST-SLPI fusion proteins was induced by the addition of 1 mM isopropyl-1-thio-β-D-galactoside, and the expressed fusion proteins were purified using glutathione-Sepharose 4B (Amersham Biosciences) according to the manufacturer's instructions. The purified proteins were incubated with PreScission Protease (Amersham Biosciences) at 4°C for 16 h to cleave the GST tag and then purified with glutathione-Sepharose 4B.

Antibacterial activity

Mid-log phase *Salmonella typhimurium* were diluted with PBS containing 1% Luria-Bertani (LB) to give $\sim 5 \times 10^7$ CFU/ml. A final volume of 250 μl was used to examine the antibacterial activities of proteins. After incubation for 2 h, *S. typhimurium* were plated onto LB agar plates. Colonies were counted (CFU/ml) after overnight incubation at 37°C.

Antimycobacterial activity

M. tuberculosis and BCG were grown in Middlebrook 7H9-ADC medium at 37°C with vigorous agitation. After 7 days of incubation, rapidly growing mycobacteria were harvested by centrifugation and adjusted to 5×10^7 CFU/ml in 7H9-ADC medium. After incubation of the mycobacteria with the indicated concentrations of proteins for 24 h at 37°C, serial 20-fold dilutions were conducted in PBS. Aliquots (50 μl) of the dilutions were plated on Middlebrook 7H10 agar plates and incubated at 37°C for 21–28 days. Colonies were counted (CFU/ml) at intervals until no new colonies appeared.

Protein-binding assay

SLPI and BSA were labeled with 5-(and 6-)carboxyfluorescein-*N*-hydroxysuccinimide ester (FLUOS; Roche Diagnostics) as described previously (30). Briefly, 400 μg/ml SLPI or BSA was mixed with 0.096 mg of FLUOS in 1 ml of PBS for 2 h at room temperature. Nonreacted FLUOS was separated by gel filtration using a Sephadex G25 column (Amersham Biosciences). The labeled SLPI or BSA was then incubated with BCG, and the OD at 630 nm was adjusted to 0.2. After 30 min of incubation at 37°C, BCG were washed three times with 7H9 medium containing 0.05% Tween 80. Protein-BCG reactions were detected by confocal laser microscopy (Zeiss).

Scanning electron microscopy

After culture with or without 1 μM SLPI for the indicated times, BCG cultures were fixed with 5% glutaraldehyde, postfixed with 1% osmium tetroxide, dehydrated with ethyl alcohol, treated with isoamyl acetate to replace the alcohol, dried with liquid CO_2 in a critical-point apparatus (HCP-2; Hitachi), and coated with Pt-Pd by ion sputtering (Hitachi) in ion-distilled water. The specimens were analyzed using S-4700 scanning electron microscope (Hitachi), operated at 10 kV.

Outer membrane permeabilization assay

The ability of proteins to permeabilize the outer membranes of BCG was investigated using 1-*N*-phenylnaphthylamine (NPN; Wako Pure Chemical Industries) as described previously (31). Briefly, BCG were suspended in 5 mM HEPES (pH 7.4) containing 10 μM NPN to an OD at 590 nm of 0.15. After incubation at 37°C for 30 min, proteins were added and the fluorescence of NPN was monitored. The excitation wavelength used was 340 nm, and the emission wavelength was 425 nm. The experiment was conducted at 37°C.

Generation of $Slpi^{-/-}$ *mice*

The *Slpi* gene was isolated from genomic DNA extracted from embryonic stem cells (E14.1) by PCR using TaKaRa LA *Taq*. The targeting vector was constructed by replacing a 1.2-kb fragment containing exons 2–4 with a neomycin-resistance gene cassette (*neo*) driven by the PGK promoter and inserting a HSV thymidine kinase into the genomic fragment for negative selection. After transfection of the targeting vector into embryonic stem cells, colonies resistant to both G418 and ganciclovir were selected and screened by PCR and Southern blotting. Homologous recombinants were microinjected into blastocysts of C57BL/6 female mice and heterozygous F_1 progenies were intercrossed to obtain $Slpi^{-/-}$ mice.

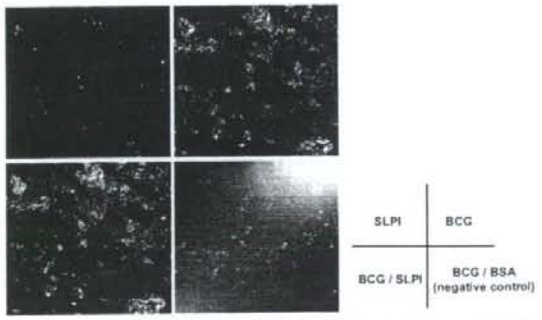

FIGURE 3. SLPI associates with BCG. SLPI and BSA were labeled with FLUOS (Roche). Labeled proteins were incubated with BCG for 30 min, and analyzed by fluorescence microscopy.

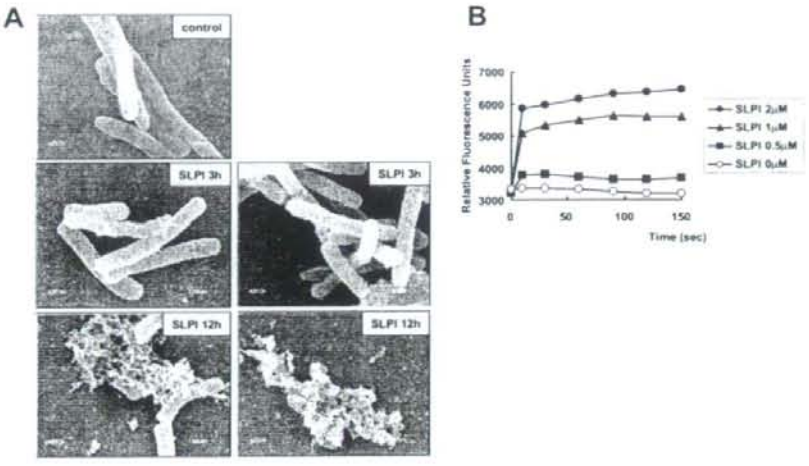

FIGURE 4. SLPI disrupts the BCG cell membrane. *A*, BCG was incubated with or without SLPI for the indicated periods and observed with scanning electron microscopy. *B*, The indicated concentrations of SLPI were added to a BCG suspension containing NPN, and the NPN fluorescence was monitored for the indicated periods. Representative data of three independent experiments are shown.

Slpi$^{-/-}$ mice were backcrossed to C57BL/6 mice for five generations, and *Slpi*$^{-/-}$ and their wild-type littermates from these intercrosses were used for experiments at 6–8 wk of age. All animal experiments were conducted in accordance with the guidelines of the Animal Care and Use Committee of Kyushu University.

In vivo infection

For intratracheal infection, 4×10^5 CFU of *M. tuberculosis* suspended in 30 μl of sterile PBS were administered intratracheally. For i.v. infection, 4×10^5 CFU of *M. tuberculosis* suspended in 100 μl of sterile PBS were administered i.v. At 3 wk after infection, homogenates of the lungs and spleen were plated on 7H10 agar plates. For histological examination, 1×10^7 CFU of *M. tuberculosis* suspended in 30 μl of sterile PBS were administered intratracheally. At 5 days after infection, the lungs were fixed in 4% formalin, embedded in paraffin, cut into sections, and stained with H&E.

Results

SLPI expression in the lungs of BCG-infected mice

To assess the roles of SLPI in mycobacterial infection, we first analyzed SLPI expression in the lungs of mice intratracheally infected with *M. bovis* BCG. Total RNA was extracted from the lungs after 2, 7, and 14 days of infection and analyzed for SLPI mRNA expression by real-time qPCR (Fig. 1*A*). Expression of SLPI mRNA was increased by ~9-fold after 2 days of infection, but decreased thereafter. Next, we analyzed pulmonary cell types expressing SLPI by immunohistochemical analysis (Fig. 1, *B* and *C*). SLPI was detected in bronchial epithelial cells before BCG infection (Fig. 1*B*, *upper micrograph*). After 2 days of BCG infection, increased amounts of SLPI expression were observed, and mainly localized at the apical side of bronchial epithelial cells (Fig. 1*B*, *lower micrograph*). This prompted us to investigate whether SLPI was secreted into the alveolar space after BCG infection. Accordingly, BALF was collected from BCG-infected mice and analyzed for SLPI protein expression by Western blotting (Fig. 1*D*). SLPI was not detected in BALF from uninfected mice. After 2 days of BCG infection, SLPI was abundantly detected in BALF from infected mice, indicating that SLPI was secreted into the alveolar space during the early phase of mycobacterial infection. In addition to bronchial epithelial cells, SLPI was expressed in cells of the alveolar area (Fig. 1*C*). Therefore, we isolated type II alveolar epithelial cells (AEC) and alveolar macrophages and analyzed their SLPI expression levels after BCG infection. Since AEC are difficult to culture in vitro, we took advantage of transgenic mice harboring a temperature-sensitive mutation of the SV40 large tumor Ag gene under the control of an IFN-γ-inducible H-2K^b promoter element (32, 33). Using these mice, we successfully established AEC lines expressing surfactant protein C (data not shown).

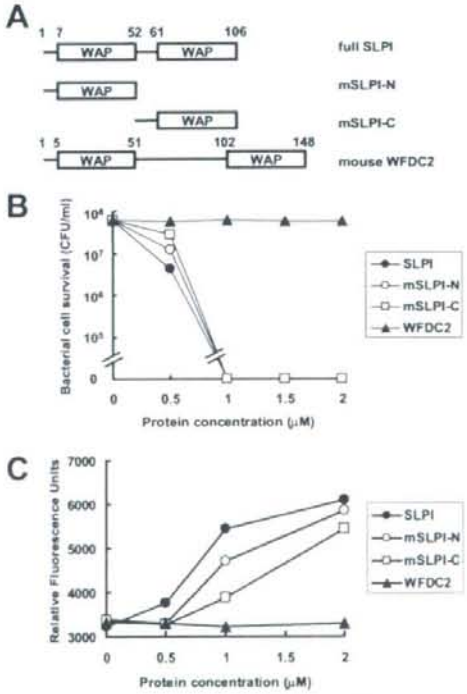

FIGURE 5. A single WAP domain in SLPI is sufficient to inhibit BCG growth. *A*, The deletion mutant constructs mSLPI-N and mSLPI-C lack the C-terminal and N-terminal portions, respectively. White boxes denote WAP domains. *B*, BCG (5×10^7 CFU/ml) was incubated with increasing concentrations of the deletion mutants (mSLPI-N and mSLPI-C) or WFDC2 for 24 h and then plated on 7H10 agar plates. *C*, The indicated concentrations of the deletion mutants (mSLPI-N and mSLPI-C) or WFDC2 were added to BCG suspensions containing NPN. The peak of NPN fluorescence within 150 s was plotted. Representative data of three independent experiments are shown.

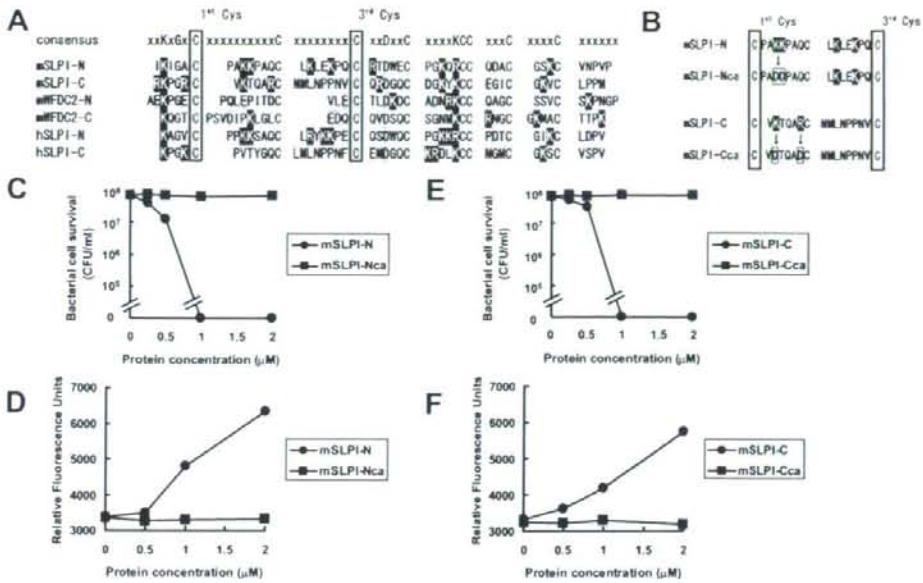

FIGURE 6. Cationic amino acids are responsible for the antimycobacterial activity of SLPI. *A*, Comparison of the WAP domain of SLPI with the WAP domains of other proteins. The consensus amino acid sequence of the WAP domain is shown at the *top* of the protein sequences. Black- and gray-boxed amino acids indicate cationic and anionic amino acids, respectively. Two conserved cysteine residues (first cysteine and third cysteine) are boxed. *B*, Amino acid sequences of the mSLPI-N (mSLPI-Nca) and mSLPI-C (mSLPI-Cca) mutants. *C* and *E*, BCG (5×10^7 CFU/ml) was incubated with increasing concentrations of mSLPI-Nca (*C*) and mSLPI-Cca (*E*) for 24 h and then plated on 7H10 agar plates. *D* and *F*, The indicated concentrations of mSLPI-Nca (*D*) and mSLPI-Cca (*F*) were added to BCG cultures containing NPN. The peak of NPN fluorescence within 150 s was plotted.

AEC were infected with BCG and analyzed for SLPI mRNA expression (Fig. 1*E*). SLPI mRNA expression was gradually induced after BCG infection and peaked after 36 h of infection. AEC have the ability to secrete several effector molecules into the alveolar space. Therefore, we analyzed the SLPI protein levels in culture supernatants from BCG-infected AEC by Western blotting (Fig. 1*F*). SLPI protein was not detected in supernatants from uninfected AEC, but was clearly detected in supernatants after 24 h of BCG infection. Next, isolated alveolar macrophages were infected with BCG and analyzed for SLPI mRNA expression (Fig. 1*G*). BCG infection resulted in an increase in SLPI mRNA expression. Taken together, mycobacterial infection induces the production and secretion of SLPI into the alveolar space by bronchial and type II alveolar epithelial cells as well as alveolar macrophages in the lung.

SLPI-mediated inhibition of mycobacterial growth

Several previous reports have described antimicrobial activities of SLPI against Gram-positive bacteria, Gram-negative bacteria, HIV, and fungi (18–20). However, SLPI needs to be present at high concentrations (>10 μM) for effective inhibition of microbial growth, particularly *S. typhimurium* and *E. coli* (18, 34). Indeed, addition of 2 μM recombinant mouse SLPI only moderately decreased the growth of *S. typhimurium* (Fig. 2*A*). In sharp contrast to the mild inhibition of *S. typhimurium* growth, addition of lower concentrations of mouse SLPI to BCG cultures dramatically reduced the number of CFU (Fig. 2*B*). Growth of BCG was almost completely inhibited by the addition of 1 μM SLPI. A similar inhibitory effect was observed on the growth of *M. tuberculosis* H37Ra and H37Rv (Fig. 2, *C* and *D*). These findings indicate that SLPI has a more potent antimicrobial activity against mycobacteria than against *S. typhimurium*.

Disruption of the BCG cell wall structure by SLPI

Next, we investigated the mechanism of the antimycobacterial activity of SLPI. First, fluorescence-labeled SLPI was incubated with BCG and analyzed by confocal laser microscopy (Fig. 3). BCG and labeled SLPI were colocalized, suggesting that SLPI becomes associated with BCG. We then examined the morphological effects of SLPI on BCG. BCG was incubated with or without SLPI and analyzed by scanning electron microscopy (Fig. 4*A*). BCG exposed to SLPI for 3 h showed pronounced surface blebbing. After 12 h of incubation, many of BCG were collapsed and few live BCG had rough and irregular membrane surfaces. Next, BCG was subjected to an outer membrane permeabilization assay using a fluorescent dye that is weakly fluorescent in aqueous environments but becomes strongly fluorescent in the hydrophobic environment within the cell membrane (Fig. 4*B*). Addition of SLPI caused rapid increases in fluorescence in a dose-dependent manner. These results suggest that SLPI directly associates with mycobacteria, and disrupts the cell wall structure.

Critical role of cationic amino acids in SLPI in its antimycobacterial activity

We next investigated the critical domain involved in the antimycobacterial activity of SLPI. SLPI has two WAP domains (Fig. 5*A*). Several serine protease inhibitors possessing a single WAP domain, such as Eppin, Elafin, SWAM1, and SWAM2, have antimicrobial activities against bacteria such as *E. coli* and *Staphylococcus aureus* (8, 21, 22). To investigate whether each of the WAP domains of mouse SLPI is sufficient to exert antimycobacterial activity, two deletion mutants of SLPI, mSLPI-N and

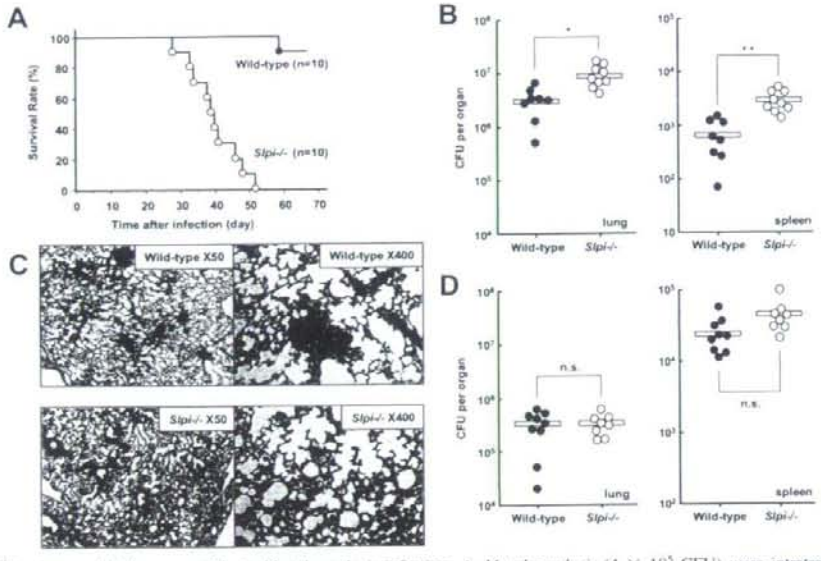

FIGURE 7. *Slpi*$^{-/-}$ mice are highly susceptible to *M. tuberculosis* infection. *A*, *M. tuberculosis* (4×10^5 CFU) were intratracheally infected into wild-type and *Slpi*$^{-/-}$ mice and their survival was monitored. *B*, *M. tuberculosis* (4×10^5 CFU) were intratracheally infected into wild-type and *Slpi*$^{-/-}$ mice. At 3 wk after infection, homogenates of the lungs and spleen were plated on 7H10 agar plates and the CFU titers were counted. Symbols represent individual mice and bars represent the mean of CFU numbers. Statistical analyses were performed using Student's *t* test: *, $p < 0.005$ and **, $p < 0.0005$, significant difference between wild-type and *Slpi*$^{-/-}$ mice. *C*, H&E staining of representative lung tissues from wild-type and *Slpi*$^{-/-}$ mice on day 5 after intratracheal infection with *M. tuberculosis*. *D*, *M. tuberculosis* (4×10^5 CFU) were i.v. infected into wild-type and *Slpi*$^{-/-}$ mice. At 3 wk after infection, homogenates of the lungs and spleen were plated on 7H10 agar plates, and the CFU titers were counted. Symbols represent individual mice and bars represent the mean of CFU numbers. Statistical analyses were performed using Student's *t* test. n.s., Not significant.

mSLPI-C, were generated (Fig. 5*A*). mSLPI-N contained the N-terminal WAP domain, while mSLPI-C contained the C-terminal WAP domain. Both mSLPI-N and mSLPI-C inhibited BCG growth, although their efficiencies were slightly decreased compared with that of full-length SLPI (Fig. 5*B*). Similarly, mSLPI-N and mSLPI-C both induced permeabilization of the outer membrane of BCG with slightly lower efficacies (Fig. 5*C*). These results imply that each WAP domain of mouse SLPI exhibits antimycobacterial activity by disrupting the mycobacterial cell wall structure. WFDC2 is a secreted protein possessing two WAP domains (Fig. 5*A*) (35). However, recombinant mouse WFDC2 had no effect on mycobacterial growth and did not induce permeabilization of the BCG cell membrane, indicating that not all WAP domain-containing proteins have antimicrobial activities (Fig. 5, *B* and *C*). In addition, the N-terminal, but not the C-terminal, WAP domain of human SLPI has been shown to mediate its antimicrobial activities against *E. coli* and *S. aureus* (18). Therefore, we compared the amino acid sequences of the WAP domains of mouse and human SLPI as well as mouse WFDC2 (Fig. 6*A*). The C-terminal regions were conserved among all of the WAP domains. However, the sequences between the first and third cysteine residues were less conserved. In particular, when we examined the sequences between the first and second cysteine residues, we noted that the WAP domains possessing antimycobacterial activities (mSLPI-N, mSLPI-C, and hSLPI-N) contained two or more cationic amino acids, whereas the WAP domains with no antimycobacterial activities (mWFDC2-N, mWFDC2-C, and hSLPI-C) had one or zero cationic acids and instead contained anionic amino acids. Therefore, we produced mSLPI-N (mSLPI-Nca) and mSLPI-C (mSLPI-Cca) mutants, in which the two cationic amino acids were changed to the anionic amino acid aspartic acid (Fig. 6*B*). Neither mSLPI-Nca nor mSLPI-Cca was able to inhibit BCG growth or permeabilize the cell membrane (Fig. 6, *C–F*). These results suggest that the cationic acids of mouse SLPI are responsible for its potent antimycobacterial activities.

High susceptibility of SLPI-deficient mice to M. tuberculosis *infection*

In the next experiment, we assessed the physiological roles of SLPI during mycobacterial infection by generating mice lacking SLPI (*Slpi*$^{-/-}$ mice) via gene targeting (data not shown). First, wild-type and *Slpi*$^{-/-}$ mice were intratracheally infected with *M. tuberculosis* H37Ra, and monitored for their survival (Fig. 7*A*). All *Slpi*$^{-/-}$ mice died within 8 wk of infection at a dose that almost all wild-type mice survived for >9 wk. Next, we counted CFU numbers in the lungs and spleen after 3 wk of infection (Fig. 7*B*). The CFU titers of *M. tuberculosis* in both tissues were higher for *Slpi*$^{-/-}$ mice than that for wild-type mice. The histopathological changes in the lungs after 5 days of *M. tuberculosis* infection were also analyzed (Fig. 7*C*). In wild-type mice, the formation of several small granulomas was observed. In contrast, granulomatous changes were induced to a lesser extent in *Slpi*$^{-/-}$ mice and rather diffuse cell infiltration was observed instead. Next, mice were i.v. infected with *M. tuberculosis*, and the CFU numbers in the lungs and spleen were counted after 3 wk of infection (Fig. 7*D*). The CFU titers were not as dramatically increased in both tissues of *Slpi*$^{-/-}$ mice compared with the corresponding titers in the tissues of wild-type mice, indicating that *Slpi*$^{-/-}$ mice are not highly susceptible to i.v. *M. tuberculosis* infection. Taken together, these findings indicate that *Slpi*$^{-/-}$ mice are highly vulnerable to *M. tuberculosis* infection via the respiratory route.

Discussion

In the present study, we analyzed the roles of mouse SLPI in host defense against mycobacteria. During the early phase of respiratory mycobacterial infection, SLPI was produced and secreted into the alveolar space by bronchial and type II alveolar epithelial cells as well as alveolar macrophages. Recombinant mouse SLPI inhibited the growth of mycobacteria more effectively than it inhibited the growth of Gram-negative bacteria. The SLPI-mediated inhibition of mycobacterial growth was attributable to disruption of the mycobacterial cell wall structure. Furthermore, *Slpi*$^{-/-}$ mice were highly susceptible to pulmonary *M. tuberculosis* infection, highlighting a mandatory role for mouse SLPI in the host defense against *M. tuberculosis* infection. Thus, mouse SLPI is a critical antimycobacterial molecule that acts during the early phase of mycobacterial infection at the respiratory mucosal surface.

Similar structural changes to those observed in SLPI-treated mycobacterial cell walls were induced in several bacteria and *M. tuberculosis* treated with the antimicrobial peptides defensins, which permeabilize microbial membranes (36, 37). We further identified the critical elements for the potent antimycobacterial activity of mouse SLPI. It has been proposed that defensins containing positively charged amino acid residues associate with microorganisms by targeting the surface-exposed negatively charged phospholipid head groups in the microbial membrane (37). Indeed, mutations that change arginine to aspartic acid can attenuate the bactericidal activity of the α-defensin cryptdin-4 (38). Therefore, we supposed that SLPI, which has similar effects on mycobacterial membranes to defensins, also associates with negatively charged mycobacterial membranes through its positively charged amino acid residues. Consistent with this hypothesis, the sequences between the first and second conserved cysteine residues of the WAP domains are not conserved. Moreover, there are several positively charged amino acids (lysine and arginine) in these regions of the WAP domains that possess antimicrobial activities, whereas the regions without any antimicrobial activities contain one or zero positively charged amino acids. Furthermore, structural studies have revealed that the region between the first and second conserved cysteine residues is exposed on the outside of the molecule, thereby enabling this region to associate with microbial membranes (39, 40). Indeed, mutations of the cationic amino acid residues within this region resulted in elimination of the antimycobacterial activity. Thus, mouse SLPI exhibits antimycobacterial activity in quite a similar manner to that of defensins.

In comparison to SLPI, higher concentrations of other serine protease inhibitors containing a WAP domain are required to inhibit microbial growth (8, 21, 22). Recombinant human SLPI is less effective at inhibiting the growth of mycobacteria and *S. typhimurium* (our unpublished data). These differential properties may be attributable to structural differences in the WAP domains, which mediate the antimicrobial activity. SLPI has two WAP domains, whereas other serine protease inhibitors, such as Eppin, Elafin, and SWAMs, have only a single WAP domain. In the case of human SLPI, only the N-terminal WAP domain exhibits antimicrobial activity (18). In addition, only the N-terminal WAP domain of human SLPI contains critical cationic acid residues. The presence of two WAP domains possessing antimicrobial activity may be responsible for the high potency of mouse SLPI for mycobacterial growth inhibition.

Mouse SLPI inhibited mycobacterial growth at profoundly lower concentrations than those required to inhibit the growth of *S. typhimurium* or other microorganisms (18–20). It remains unclear how SLPI becomes more specifically targeted toward mycobacteria. Differential antimicrobial properties against distinct microorganisms have not been reported in the case of defensins. Therefore, SLPI, which has multifunctional properties, may have an unknown strategy for specifically recognizing mycobacteria.

The in vitro findings demonstrating that mouse SLPI inhibits mycobacterial growth were further strengthened by in vivo studies using *Slpi*$^{-/-}$ mice. *Slpi*$^{-/-}$ mice were highly susceptible to pulmonary *M. tuberculosis* infection, but not to i.v. infection. In accordance with this finding, SLPI protein was abundantly detected in the alveolar space after pulmonary BCG infection, but was not detected in sera from mice after i.v. BCG infection (our unpublished data). Therefore, high concentrations of SLPI are supposed to be secreted into the alveolar space during the early phase of respiratory infection with *M. tuberculosis*, thereby promptly killing the mycobacteria before they can invade the lung tissues through the epithelial barrier. Given that mouse SLPI has potent antimycobacterial activities, it would be a good candidate for treatment during the acute phase of *M. tuberculosis* infection and may even be able to be used for the treatment of patients with multidrug-resistant *M. tuberculosis*.

Acknowledgments

We thank S. Ehrt and A. Ding for helpful discussions, Y. Yamada and K. Takeda for technical assistance, and M. Kurata for secretarial assistance.

Disclosures

The authors have no financial conflict of interest.

References

1. Kaufmann, S. H. 2006. Tuberculosis: back on the immunologists' agenda. *Immunity* 24: 351–357.
2. North, R. J., and Y. J. Jung. 2004. Immunity to tuberculosis. *Annu. Rev. Immunol.* 22: 599–623.
3. Fremond, C. M., V. Yeremeev, D. M. Nicolle, M. Jacobs, V. F. Quesniaux, and B. Ryffel. 2004. Fatal *Mycobacterium tuberculosis* infection despite adaptive immune response in the absence of MyD88. *J. Clin. Invest.* 114: 1790–1799.
4. Quesniaux, V., C. Fremond, M. Jacobs, S. Parida, D. Nicolle, V. Yeremeev, F. Bihl, F. Erard, T. Botha, M. Drennan, et al. 2004. Toll-like receptor pathways in the immune responses to mycobacteria. *Microbes Infect.* 6: 946–959.
5. Gerritsen, J. 2000. Host defence mechanisms of the respiratory system. *Paediatr. Respir. Rev.* 1: 128–134.
6. Clauss, A., H. Lilja, and A. Lundwall. 2005. The evolution of a genetic locus encoding small serine proteinase inhibitors. *Biochem. Biophys. Res. Commun.* 333: 383–389.
7. Eisenberg, S. P., K. K. Hale, P. Heimdal, and R. C. Thompson. 1990. Location of the protease-inhibitory region of secretory leukocyte protease inhibitor. *J. Biol. Chem.* 265: 7976–7981.
8. Hagiwara, K., T. Kikuchi, Y. Endo, Huqun, K. Usui, M. Takahashi, N. Shibata, T. Kusakabe, H. Xin, S. Hoshi, et al. 2003. Mouse SWAM1 and SWAM2 are antibacterial proteins composed of a single whey acidic protein motif. *J. Immunol.* 170: 1973–1979.
9. Abe, T., N. Kobayashi, K. Yoshimura, B. C. Trapnell, H. Kim, R. C. Hubbard, M. T. Brewer, R. C. Thompson, and R. G. Crystal. 1991. Expression of the secretory leukoprotease inhibitor gene in epithelial cells. *J. Clin. Invest.* 87: 2207–2215.
10. Hiemstra, P. S., S. van Wetering, and J. Stolk. 1998. Neutrophil serine proteinases and defensins in chronic obstructive pulmonary disease: effects on pulmonary epithelium. *Eur. Respir. J.* 12: 1200–1208.
11. Schiessler, H., E. Fink, and H. Fritz. 1976. Acid-stable proteinase inhibitors from human seminal plasma. *Methods Enzymol.* 45: 847–859.
12. Vogelmeier, C., R. C. Hubbard, G. A. Fells, H. P. Schnebli, R. C. Thompson, H. Fritz, and R. G. Crystal. 1991. Anti-neutrophil elastase defense of the normal human respiratory epithelial surface provided by the secretory leukoprotease inhibitor. *J. Clin. Invest.* 87: 482–488.
13. Wingens, M., B. H. van Bergen, P. S. Hiemstra, J. F. Meis, I. M. van Vlijmen-Willems, P. L. Zeeuwen, J. Mulder, H. A. Kramps, F. van Ruissen, and J. Schalkwijk. 1998. Induction of SLPI (ALP/HUSI-I) in epidermal keratinocytes. *J. Invest. Dermatol.* 111: 996–1002.
14. Gauthier, F., U. Fryksmark, K. Ohlsson, and J. G. Bieth. 1982. Kinetics of the inhibition of leukocyte elastase by the bronchial inhibitor. *Biochim. Biophys. Acta* 700: 178–183.
15. Thompson, R. C., and K. Ohlsson. 1986. Isolation, properties, and complete amino acid sequence of human secretory leukocyte protease inhibitor, a potent inhibitor of leukocyte elastase. *Proc. Natl. Acad. Sci. USA* 83: 6692–6696.
16. Ashcroft, G. S., K. Lei, W. Jin, G. Longenecker, A. B. Kulkarni, T. Greenwell-Wild, H. Hale-Donze, G. McGrady, X. Y. Song, and S. M. Wahl. 2000. Secretory leukocyte protease inhibitor mediates non-redundant functions necessary for normal wound healing. *Nat. Med.* 6: 1147–1153.

17. Zhu, J., C. Nathan, W. Jin, D. Sim, G. S. Ashcroft, S. M. Wahl, L. Lacomis, H. Erdjument-Bromage, P. Tempst, C. D. Wright, and A. Ding. 2002. Conversion of proepithelin to epithelins: roles of SLPI and elastase in host defense and wound repair. *Cell* 111: 867–878.
18. Hiemstra, P. S., R. J. Maassen, J. Stolk, R. Heinzel-Wieland, G. J. Steffens, and J. H. Dijkman. 1996. Antibacterial activity of antileukoprotease. *Infect. Immun.* 64: 4520–4524.
19. McNeely, T. B., D. C. Shugars, M. Rosendahl, C. Tucker, S. P. Eisenberg, and S. M. Wahl. 1997. Inhibition of human immunodeficiency virus type 1 infectivity by secretory leukocyte protease inhibitor occurs prior to viral reverse transcription. *Blood* 90: 1141–1149.
20. Tomee, J. F., P. S. Hiemstra, R. Heinzel-Wieland, and H. F. Kauffman. 1997. Antileukoprotease: an endogenous protein in the innate mucosal defense against fungi. *J. Infect. Dis.* 176: 740–747.
21. Simpson, A. J., A. I. Maxwell, J. R. Govan, C. Haslett, and J. M. Sallenave. 1999. Elafin (elastase-specific inhibitor) has anti-microbial activity against Gram-positive and Gram-negative respiratory pathogens. *FEBS Lett.* 452: 309–313.
22. Yenugu, S., R. T. Richardson, P. Sivashanmugam, Z. Wang, M. G. O'Rand, F. S. French, and S. H. Hall. 2004. Antimicrobial activity of human EPPIN, an androgen-regulated, sperm-bound protein with a whey acidic protein motif. *Biol. Reprod.* 71: 1484–1490.
23. Jin, F. Y., C. Nathan, D. Radzioch, and A. Ding. 1997. Secretory leukocyte protease inhibitor: a macrophage product induced by and antagonistic to bacterial lipopolysaccharide. *Cell* 88: 417–426.
24. Taggart, C. C., S. A. Cryan, S. Weldon, A. Gibbons, C. M. Greene, E. Kelly, T. B. Low, S. J. O'Neill, and N. G. McElvaney. 2005. Secretory leucoprotease inhibitor binds to NF-κB binding sites in monocytes and inhibits p65 binding. *J. Exp. Med.* 202: 1659–1668.
25. Taggart, C. C., C. M. Greene, N. G. McElvaney, and S. O'Neill. 2002. Secretory leucoprotease inhibitor prevents lipopolysaccharide-induced IκBα degradation without affecting phosphorylation or ubiquitination. *J. Biol. Chem.* 277: 33648–33653.
26. Nakamura, A., Y. Mori, K. Hagiwara, T. Suzuki, T. Sakakibara, T. Kikuchi, T. Igarashi, M. Ebina, T. Abe, J. Miyazaki, et al. 2003. Increased susceptibility to LPS-induced endotoxin shock in secretory leukoprotease inhibitor (SLPI)-deficient mice. *J. Exp. Med.* 197: 669–674.
27. Ding, A., H. Yu, J. Yang, S. Shi, and S. Ehrt. 2005. Induction of macrophage-derived SLPI by *Mycobacterium tuberculosis* depends on TLR2 but not MyD88. *Immunology* 116: 381–389.
28. Doi, T., H. Yamada, T. Yajima, W. Wajjwalku, T. Hara, and Y. Yoshikai. 2007. H2-M3-restricted $CD8^+$ T cells induced by peptide-pulsed dendritic cells confer protection against *Mycobacterium tuberculosis*. *J. Immunol.* 178: 3806–3813.
29. deMello, D. E., S. Mahmoud, P. J. Padfield, and J. W. Hoffmann. 2000. Generation of an immortal differentiated lung type-II epithelial cell line from the adult H-$2K^b$tsA58 transgenic mouse. *In Vitro Cell. Dev. Biol. Anim.* 36: 374–382.
30. Aoki, K., S. Matsumoto, Y. Hirayama, T. Wada, Y. Ozeki, M. Niki, P. Domenech, K. Umemori, S. Yamamoto, A. Mineda, et al. 2004. Extracellular mycobacterial DNA-binding protein 1 participates in mycobacterium-lung epithelial cell interaction through hyaluronic acid. *J. Biol. Chem.* 279: 39798–39806.
31. Loh, B., C. Grant, and R. E. Hancock. 1984. Use of the fluorescent probe 1-*N*-phenylnaphthylamine to study the interactions of aminoglycoside antibiotics with the outer membrane of *Pseudomonas aeruginosa*. *Antimicrob. Agents Chemother.* 26: 546–551.
32. Jat, P. S., M. D. Noble, P. Ataliotis, Y. Tanaka, N. Yannoutsos, L. Larsen, and D. Kioussis. 1991. Direct derivation of conditionally immortal cell lines from an H-$2K^b$-tsA58 transgenic mouse. *Proc. Natl. Acad. Sci. USA* 88: 5096–5100.
33. Whitehead, R. H., P. E. VanEeden, M. D. Noble, P. Ataliotis, and P. S. Jat. 1993. Establishment of conditionally immortalized epithelial cell lines from both colon and small intestine of adult H-$2K^b$-tsA58 transgenic mice. *Proc. Natl. Acad. Sci. USA* 90: 587–591.
34. Si-Tahar, M., D. Merlin, S. Sitaraman, and J. L. Madara. 2000. Constitutive and regulated secretion of secretory leukocyte proteinase inhibitor by human intestinal epithelial cells. *Gastroenterology* 118: 1061–1071.
35. Kirchhoff, C., I. Habben, R. Ivell, and N. Krull. 1991. A major human epididymis-specific cDNA encodes a protein with sequence homology to extracellular proteinase inhibitors. *Biol. Reprod.* 45: 350–357.
36. Miyakawa, Y., P. Ratnakar, A. G. Rao, M. L. Costello, O. Mathieu-Costello, R. I. Lehrer, and A. Catanzaro. 1996. In vitro activity of the antimicrobial peptides human and rabbit defensins and porcine leukocyte protegrin against *Mycobacterium tuberculosis*. *Infect. Immun.* 64: 926–932.
37. Zasloff, M. 2002. Antimicrobial peptides of multicellular organisms. *Nature* 415: 389–395.
38. Tanabe, H., X. Qu, C. S. Weeks, J. E. Cummings, S. Kolusheva, K. B. Walsh, R. Jelinek, T. K. Vanderlick, M. E. Selsted, and A. J. Ouellette. 2004. Structure-activity determinants in Paneth cell α-defensins: loss-of-function in mouse cryptdin-4 by charge-reversal at arginine residue positions. *J. Biol. Chem.* 279: 11976–11983.
39. Grutter, M. G., G. Fendrich, R. Huber, and W. Bode. 1988. The 2.5 A X-ray crystal structure of the acid-stable proteinase inhibitor from human mucous secretions analysed in its complex with bovine α-chymotrypsin. *EMBO J.* 7: 345–351.
40. Lin, C. C., and J. Y. Chang. 2006. Pathway of oxidative folding of secretory leucocyte protease inhibitor: an 8-disulfide protein exhibits a unique mechanism of folding. *Biochemistry* 45: 6231–6240.

Lipocalin 2-Dependent Inhibition of Mycobacterial Growth in Alveolar Epithelium[1]

Hiroyuki Saiga,*† Junichi Nishimura,* Hirotaka Kuwata,† Megumi Okuyama,* Sohkichi Matsumoto,‖ Shintaro Sato,§ Makoto Matsumoto,† Shizuo Akira,§¶ Yasunobu Yoshikai,‡ Kenya Honda,* Masahiro Yamamoto,* and Kiyoshi Takeda[2]*†¶

Mycobacterium tuberculosis **invades alveolar epithelial cells as well as macrophages. However, the role of alveolar epithelial cells in the host defense against *M. tuberculosis* remains unknown. In this study, we report that lipocalin 2 (Lcn2)-dependent inhibition of mycobacterial growth within epithelial cells is required for anti-mycobacterial innate immune responses. Lcn2 is secreted into the alveolar space by alveolar macrophages and epithelial cells during the early phase of respiratory mycobacterial infection. Lcn2 inhibits the in vitro growth of mycobacteria through sequestration of iron uptake. Lcn2-deficient mice are highly susceptible to intratracheal infection with *M. tuberculosis*. Histological analyses at the early phase of mycobacterial infection in Lcn2-deficient mice reveal increased numbers of mycobacteria in epithelial cell layers, but not in macrophages, in the lungs. Increased intracellular mycobacterial growth is observed in alveolar epithelial cells, but not in alveolar macrophages, from Lcn2-deficient mice. The inhibitory action of Lcn2 is blocked by the addition of endocytosis inhibitors, suggesting that internalization of Lcn2 into the epithelial cells is a prerequisite for the inhibition of intracellular mycobacterial growth. Taken together, these findings highlight a pivotal role for alveolar epithelial cells during mycobacterial infection, in which Lcn2 mediates anti-mycobacterial innate immune responses within the epithelial cells.** ***The Journal of Immunology,*** **2008, 181: 8521–8527.**

Tuberculosis is a worldwide disease caused by infection with *Mycobacterium tuberculosis*. Therefore, the host defense mechanisms against *M. tuberculosis* have been intensively investigated, and important roles of T cell-mediated adaptive immunity have been well established (1, 2). In addition, functional characterization of TLRs has recently indicated the importance of innate immunity in the host responses to infection with *M. tuberculosis* (3, 4). In the TLR-mediated anti-mycobacterial immune responses, macrophages and dendritic cells are major effectors that engulf pathogens and produce a variety of proinflammatory mediators. In respiratory mycobacterial infection, alveolar macrophages are the major targets of invasion. However, several evidences indicate that mycobacteria also interact with epithelial cells in the respiratory tract and invade these cells (5–9). Accordingly, epithelial cells in the lungs are expected to play a role during mycobacterial infection by producing antimicrobial mediators (10).

Lipocalin 2 (Lcn2),[3] also known as neutrophil gelatinase-associated lipocalin, siderocalin, 24p3, or uterocalin, a member of the lipocalin family of proteins that bind to small hydrophobic molecules, is produced by epithelial cells and macrophages (11–16). Lcn2 has been shown to mediate several biological processes, including mammary gland involution, induction of apoptosis, and delivery of iron (12, 17–19). In addition, structural studies have demonstrated that Lcn2 binds to enterobactin-type bacterial siderophores, which facilitate iron uptake by bacteria (16). Subsequent studies revealed that Lcn2 also binds to other types of siderophores, such as carboxy-mycobactin (produced by mycobacteria) and bacillibactin (produced by *Bacillus anthracis*) (20, 21). Lcn2 has been shown to interfere with siderophore-mediated iron uptake in *Escherichia coli* (16). Accordingly, mice deficient in Lcn2 are highly susceptible to infection with *E. coli* (22, 23). Thus, Lcn2 mediates the host defense against *E. coli* infection through sequestration of iron, which is essential for the growth and activity of nearly all bacteria (24).

Mycobacteria replicate within cells, especially in the phagosome of macrophages (25), where iron is limited. Outside host cells, free iron is also limited, because almost all iron ions exist as complexes with host proteins with high affinity for iron, such as transferrin and lactoferrin. To overcome the iron deficiency within the host, some species of mycobacteria, such as *M. tuberculosis* and *Mycobacterium bovis* bacillus Calmette-Guérin (BCG), synthesize two type of siderophores, called mycobactin and carboxy-mycobactin (also called exochelin) (26, 27). Mycobactin is hydrophobic, whereas carboxy-mycobactin is hydrophilic. These mycobactins have been shown to remove iron from host iron-binding proteins, such as transferrin and lactoferrin (28). In addition, *M. tuberculosis*

*Laboratory of Immune Regulation, Department of Microbiology and Immunology, Graduate School of Medicine, Osaka University, Suita, Osaka, Japan; †Department of Molecular Genetics and ‡Division of Host Defense, Research Center for Prevention of Infectious Diseases, Medical Institute of Bioregulation, Kyushu University, Fukuoka, Japan; §Department of Host Defense, Research Institute for Microbial Diseases and ¶WPI Immunology Frontier Research Center, Osaka University, Suita, Osaka, Japan; and ‖Department of Bacteriology, Osaka City University Graduate School of Medicine, Osaka, Japan

Received for publication August 5, 2008. Accepted for publication October 11, 2008.

The costs of publication of this article were defrayed in part by the payment of page charges. This article must therefore be hereby marked *advertisement* in accordance with 18 U.S.C. Section 1734 solely to indicate this fact.

[1] This work was supported by a Grant-in-Aid from the Ministry of Education, Culture, Sports, Science and Technology and the Ministry of Health, Labor and Welfare, as well as the Osaka Foundation for the Promotion of Clinical Immunology.

[2] Address correspondence and reprint requests to Dr. Kiyoshi Takeda, Laboratory of Immune Regulation, Department of Microbiology and Immunology, Graduate School of Medicine, Osaka University, Suita, Osaka, Japan. E-mail address: ktakeda@ongene.med.osaka-u.ac.jp

[3] Abbreviations used in this paper: Lcn2, lipocalin 2; BCG, *Mycobacterium bovis* bacillus Calmette-Guérin; BALF, bronchoalveolar lavage fluid; rLcn2, recombinant Lcn2; SP-C, pro-surfactant protein C; DFO, deferoxamine; AEC, alveolar epithelial cell; CPZ, chlorpromazine.

with mutations in the *mbtB* gene, which lack carboxy-mycobactin and mycobactin, exhibit impaired replication in low-iron medium and within macrophages (27). The mechanisms for the mycobactin-mediated iron acquisition within the phagosome of macrophages have recently been elucidated (29). Because pulmonary epithelial cells are also invaded by mycobacteria, host defense mechanisms that inhibit mycobacterial replication within these cells are expected to exist, however they currently remain unclear.

In the present study, we analyzed the role of Lcn2 in mycobacterial infection. Lcn2, which inhibits mycobacterial growth, was rapidly produced from alveolar macrophages and epithelial cells after mycobacterial infection. Furthermore, analyses using Lcn2-deficient mice revealed a pivotal role of alveolar epithelial cells in mycobacterial infection.

Materials and Methods

Mice

Lcn2$^{-/-}$ and *H-2K*^{b}*-tsA58* transgenic mice have been generated (22, 30) and backcrossed to C57BL/6 for six generations. *Lcn2*$^{-/-}$ and wild-type littermates from intercrosses of *Lcn2*$^{+/-}$ mice were used for experiments at 6–8 wk of age. All animal experiments were conducted in accordance with the guidelines of the Animal Care and Use Committee of Kyushu University and Osaka University.

Mycobacteria

M. bovis BCG (Tokyo strain) was purchased from Kyowa Pharmaceuticals. *M. tuberculosis* strains H37Ra (ATCC25177) and H37Rv (ATCC358121) were grown in Middlebrook 7H9-ADC medium for 2 wk and stored at −80°C until use. GFP-expressing BCG, which was generated previously (5), was used for the experiment.

Quantitative real-time RT-PCR

Total RNA was isolated with the TRIzol reagent (Invitrogen), and reverse transcribed using M-MLV reverse transcriptase (Promega) and random primers (Toyobo) after treatment with RQ1 DNaseI (Promega). Quantitative real-time PCR was performed in ABI7300 (Applied Biosystems) using TaqMan Universal PCR Master Mix (Applied Biosystems). All data are shown as the relative mRNA levels normalized by the corresponding 18S rRNA level. The primers for 18S rRNA and Lcn2 were purchased from Assays on Demand (Applied Biosystems).

Preparation of alveolar macrophages

Bronchoalveolar lavage fluid (BALF) was collected from uninfected mice. To eliminate contamination by bacteria, the cells were cultured with 50 U/ml penicillin and 50 μg/ml streptomycin for 16 h, and then washed five times to remove nonadherent cells. The resultant adherent cells were used for experiments as alveolar macrophages, because >95% of the adherent cells were CD11b-positive.

Preparation of recombinant Lcn2 (rLcn2) protein

A mouse Lcn2 cDNA fragment was inserted into pGEX6P-2 (GE Healthcare) and transformed into *E. coli* BL21. The expressed GST-Lcn2 fusion proteins were purified using glutathione-Sepharose 4B (GE Healthcare) according to the manufacturer's instructions. The purified proteins were incubated with PreScission Protease (GE Healthcare) to cleave the GST tag, and then purified with Glutathione-Sepharose 4B.

Immunohistochemistry

Lungs were fixed with 4% PFA and frozen in Tissue-Tec OCT compound (Sakura). The sections were incubated with anti-mouse Lcn2 Ab (R&D Systems), anti-pro-surfactant protein C (SP-C) Ab (Chemicon), anti-CD11b Ab (BD Biosciences), or anti-pan cytokeratin Ab (Sigma-Aldrich). The nuclei were stained with 4′,6-diamidino-2-phenylindole (DAPI; Molecular Probes). Alveolar epithelial cells were infected with GFP-expressing BCG for 16 h, washed, and incubated with Dextran Conjugates (Cascade Blue; Molecular Probes) and Alexa Fluor 594-labeled rLcn2 for 6 h. rLcn2 was labeled using an Alexa Fluor 594 Protein Labeling Kit (Molecular Probes). The cells were fixed with 4% PFA and analyzed using a confocal microscopy (LSM 510; Carl Zeiss).

Western blot assay

BALF was collected from BCG-infected mice by catheterization techniques into 500 μl of PBS. To normalize BALF samples, we injected the same volume of PBS (500 μl), recovered equal volume, and used them for Western blot analysis. After removal of precipitates, the samples were separated on SDS-PAGE and transferred to PVDF membranes (Millipore). The membranes were incubated with anti-mouse Lcn2 Ab. Bound Ab was detected with SuperSignal West Pico Chemiluminescent Substrate (Pierce).

In vitro mycobacterial growth assay

Mycobacteria were incubated in Middlebrook 7H9-ADC medium with the indicated concentrations of rLcn2 protein for 20 days at 37°C, and were plated on Middlebrook 7H10-OADC agar plates and incubated at 37°C for 30 days. In some experiments, BCG was incubated with the indicated concentrations of deferoxamine mesylate (DFO; Calbiochem), $FeCl_3$ or mycobactin (Kyoritsu Seiyaku) on 7H10-OADC agar plates.

In vivo infection of mycobacteria

Mice were intratracheally infected with *M. tuberculosis* H37Rv (1×10^6 CFU). At 6 wk after infection, homogenates of the lungs and livers were plated on 7H10-OADC agar plates. For histological analyses, the lungs were fixed with 4% PFA at 20 or 5 days after infection, embedded in paraffin, cut into sections, and stained with H&E or by the Ziehl-Neelsen method, respectively.

Establishment of alveolar epithelial cell lines

To establish alveolar epithelial cell lines (AECs) from wild-type and *Lcn2*$^{-/-}$ mice, the mice were crossed with *H-2K*^{b}*-tsA58* transgenic mice, and used for experiments at 4 wk of age. Mouse pulmonary type II AECs were established as previously described (32). The cells were incubated at 33°C and passaged over ten times. The cells were then stained with anti-SP-C Ab to confirm that they were type II alveolar epithelial cells.

In vitro infection of mycobacteria

Wild-type or *Lcn2*$^{-/-}$ derived AECs or alveolar macrophages were incubated with BCG for the indicated periods. To eliminate extracellular BCG, the cells were cultured with 50 μg/ml streptomycin for 1 h, washed three times, and harvested. Lysates of the cells were plated on 7H10-OADC agar plates.

Detection of intracellular growth of mycobacteria

Wild-type and *Lcn2*$^{-/-}$-derived AECs were seeded onto 96-well plates, and infected with BCG for 6 h. To eliminate extracellular BCG, the AECs were cultured with 50 μg/ml streptomycin for 1 h, vigorously washed three times. The cells were pulsed with 37 kBq of [^{3}H]uracil and cultured for 48 h. The cells were harvested on glass fiber filters and the incorporated [^{3}H]uracil was measured using a liquid scintillation counter (Wallac). In some experiments, cytochalasin B (Sigma-Aldrich) or chlorpromazine (CPZ; Calbiochem) was added to the wells at 30 min before the [^{3}H]uracil pulse or rLcn2 addition.

Statistical analysis

Differences between control and experimental groups were evaluated using Student's *t* test or ANOVA plus posthoc testing. Values of $p < 0.05$ were considered to indicate statistical significance.

Results

Expression of lipocalin 2 in BCG-infected lungs

To assess the role of Lcn2 in mycobacterial infection, we first analyzed the expression of Lcn2 in the lungs of C57BL/6 mice intratracheally infected with BCG. Total RNA was extracted from the lungs at 2, 7, and 14 days after infection, and analyzed for Lcn2 mRNA expression by real-time quantitative PCR (Fig. 1*A*). Expression of Lcn2 mRNA was markedly increased at 2 days after infection and decreased thereafter. Because Lcn2 mRNA expression was shown to be induced in macrophages stimulated with TLR ligands (22), we analyzed whether alveolar macrophages expressed Lcn2 mRNA (Fig. 1*B*). Alveolar macrophages were isolated, infected with BCG, and analyzed for Lcn2 mRNA expression at 2 days

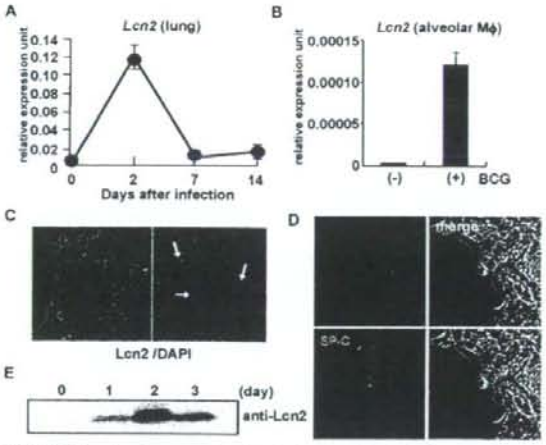

FIGURE 1. Lcn2 expression in the lungs of BCG-infected mice. *A*, Wild-type C57BL/6 mice were intratracheally infected with 2.5×10^6 CFU of BCG. Total RNA was extracted from the lungs after the indicated periods. Lcn2 mRNA expression was analyzed by real-time quantitative PCR. Data are shown as the relative mRNA levels normalized by the corresponding 18S rRNA level. Data are presented as means ± SD, and are representative of two independent experiments. *B*, Alveolar macrophages were isolated from uninfected wild-type mice, cultured with or without BCG for 48 h, and then analyzed for their Lcn2 mRNA expression by real-time quantitative PCR. *C* and *D*, At 2 days after intratracheal infection with BCG, lung tissue sections were stained with anti-Lcn2 Ab (red), DAPI (blue), and anti-SP-C Ab (green), and visualized by fluorescence microscopy. *E*, Wild-type mice were intratracheally infected with 2.5×10^6 CFU of BCG. At the indicated time points after the infection, 500 μl of PBS was intratracheally injected and then recovered. The recovered BALF samples were subjected to Western blot analysis with anti-Lcn2 Ab.

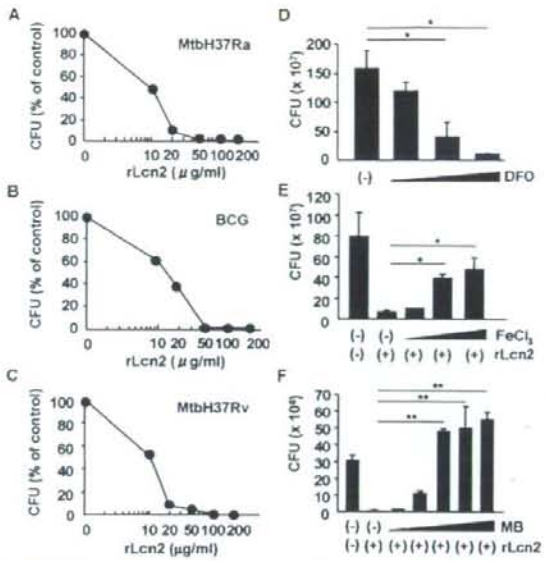

FIGURE 2. Inhibition of in vitro mycobacterial growth by Lcn2. *A–C*, *M. tuberculosis* H37Ra (*A*), BCG (*B*), or *M. tuberculosis* H37Rv (*C*) (1×10^6 CFU each) was incubated with the indicated concentrations of rLcn2 in 7H9 ADC medium for 20 days and then plated on 7H10-OADC agar. The CFU numbers were counted. *D*, BCG was incubated with increasing concentrations of DFO (1 μM, 100 μM and 1 mM) for 20 days and then plated on 7H10-OADC agar. The CFU numbers were counted. *E* and *F*, BCG was incubated in the presence of rLcn2 (50 μg/ml) as well as increasing concentrations of $FeCl_3$ (*E*: 5 nM, 500 nM, 50 μM, and 5 mM) or MB (*F*: 1 pg/ml, 10 pg/ml, 1 ng/ml, 100 ng/ml, and 10 μg/ml) (*F*) for 20 days, and then plated on 7H10-OADC agar. All data are presented as means ± SD. * and ** indicate a significant difference among groups, ANOVA, posthoc Scheffe; *, $p < 0.05$; **, $p < 0.005$.

after infection; BCG infection led to a marked increase in the expression of Lcn2 mRNA. We also analyzed the lungs by immunohistochemistry using an anti BCG-infected mice, several Lcn2-positive cells were observed. These cells mainly faced the alveolar surface and projected into the alveolar space, representing the typical morphology of type II alveolar epithelial cells. Costaining with an Ab to pro-SP-C, which is produced by type II alveolar epithelial cells, revealed that both Lcn2 and SP-C were produced by the same cells (Fig. 1*D*). These findings indicate that not only alveolar macrophages but also type II alveolar epithelial cells produce Lcn2 during respiratory mycobacterial infection. Type II alveolar epithelial cells are known to secrete several mediators into the alveolar space. Therefore, we analyzed whether Lcn2 is secreted into the alveolar space during intratracheal BCG infection. BALF was collected from uninfected and BCG-infected mice and analyzed for Lcn2 protein expression by Western blotting (Fig. 1*E*). Lcn2 was not detected in BALF from uninfected mice. At 2 days after BCG infection, Lcn2 expression was abundantly detected in BALF from the infected mice, indicating that Lcn2 was secreted into the alveolar space during the early phase of mycobacterial infection.

Lcn2-mediated inhibition of mycobacterial growth

We produced rLcn2 and analyzed its effect on in vitro mycobacterial growth. Addition of rLcn2 dose-dependently inhibited the growth of avirulent strains of mycobacteria such as BCG and *M. tuberculosis* H37Ra (Fig. 2, *A* and *B*). rLcn2 also inhibited the growth of virulent *M. tuberculosis* H37Rv in a dose-dependent manner (Fig. 2*C*). Thus, Lcn2 has the ability to inhibit the growth of several mycobacterial strains.

We investigated whether Lcn2 inhibits mycobacterial growth by interfering with iron acquisition, similar to the case for inhibition of *E. coli* growth (16). First, we added DFO, an iron chelator, into in vitro BCG cultures (Fig. 2*D*). DFO reduced BCG growth in a dose-dependent manner, indicating that BCG requires iron for growth. Next, we added ferric iron into BCG cultures (Fig. 2*E*). Addition of ferric iron rescued Lcn2-mediated inhibition of BCG growth in a dose-dependent manner, indicating that Lcn2 inhibits use of iron from the culture medium. Addition of exogenous mycobactin (MB) also abolished Lcn2-mediated inhibition of BCG growth (Fig. 2*F*). These findings indicate that Lcn2 inhibits mycobacterial growth by sequestering iron.

In vivo anti-mycobacterial activity of lipocalin 2

We next addressed the in vivo role of Lcn2 in *M. tuberculosis* infection using $Lcn2^{-/-}$ mice. Wild-type and $Lcn2^{-/-}$ mice were intratracheally infected with *M. tuberculosis* H37Rv and monitored for their survival (Fig. 3*A*). $Lcn2^{-/-}$ mice were highly sensitive to intratracheal infection with *M. tuberculosis* and many of the infected mice died. We also counted the CFU numbers in the lungs and livers after 6 wk of infection (Fig. 3*B*). The CFU titer of *M. tuberculosis* was higher in $Lcn2^{-/-}$ mice than that in wild-type mice. Histopathological analysis of the lungs of the infected mice at 20 days after infection revealed that the number and size of the granulomatous lesions were increased in $Lcn2^{-/-}$ mice (Fig. 3*C*), indicating that the inflammatory response in $Lcn2^{-/-}$ mice was enhanced, possibly due to progression of the *M. tuberculosis* infection. These findings demonstrate that Lcn2 plays an important role in host resistance to *M. tuberculosis* infection in vivo.

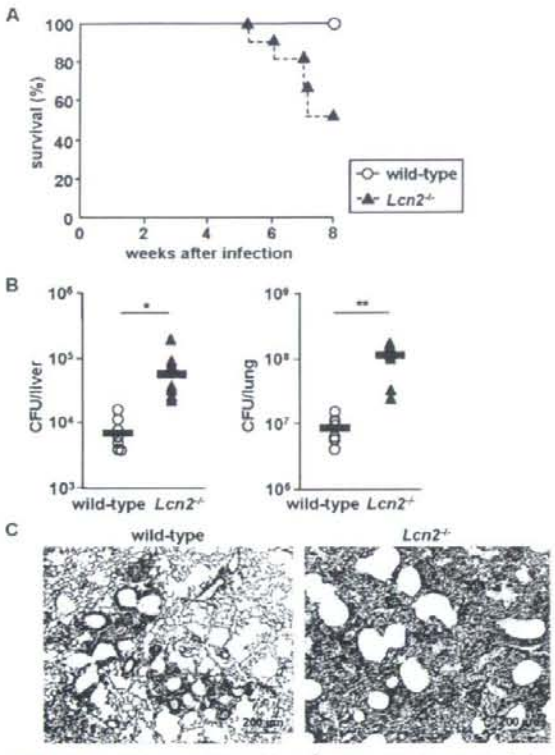

FIGURE 3. High susceptibility of *Lcn2*$^{-/-}$ mice to *M. tuberculosis* infection. *A*, Wild-type ($n = 11$) and *Lcn2*$^{-/-}$ ($n = 12$) mice were intratracheally infected with *M. tuberculosis* H37Rv (1×10^6 CFU) and their survival was monitored for 8 wk. *B*, Wild-type ($n = 7$) and *Lcn2*$^{-/-}$ ($n = 7$) mice were intratracheally infected with *M. tuberculosis* H37Rv (1×10^6 CFU). At 6 wk after infection, homogenates of the lungs and livers were plated on 7H10-OADC agar and the CFU titers were counted. Symbols represent individual mice, and bars represent the mean CFU numbers. *, $p < 0.05$; **, $p < 0.005$. Data are representative of two independent experiments. *C*, H&E staining of representative lung tissues from wild-type and *Lcn2*$^{-/-}$ mice at 20 days after intratracheal infection with *M. tuberculosis*.

Increased numbers of mycobacteria in Lcn2-deficient alveolar epithelial cells

We next analyzed the localization of *M. tuberculosis* in the lungs at 5 days after intratracheal infection by staining acid-fast bacilli using the Ziehl-Neelsen method. In wild-type and *Lcn2*$^{-/-}$ mice, similar densities of *M. tuberculosis* were observed in granulomatous lesions, although the number and size of the granulomatous lesions were increased in *Lcn2*$^{-/-}$ mice (data not shown). In addition, *M. tuberculosis* exhibited similar staining of cells with a macrophage-like morphology in wild-type and *Lcn2*$^{-/-}$ mice (Fig. 4*A*). Strikingly, some of the alveolar epithelial cell layers in *Lcn2*$^{-/-}$ mice contained *M. tuberculosis* (Fig. 4*B*). In sharp contrast, *M. tuberculosis* was scarcely detected within the epithelial cell layers of wild-type mice. To corroborate these findings, we subjected the lungs of mice intratracheally infected with GFP-expressing BCG to immunohistochemical analyses. In both wild-type and *Lcn2*$^{-/-}$ mice, CD11b-positive cells contained GFP-expressing BCG. However, in the lungs of *Lcn2*$^{-/-}$ mice, GFP-expressing BCG was frequently observed in cells that did not express CD11b, in contrast to the low frequency observed in the lungs of wild-type mice (Fig. 4*C*). Visualization of epithelial cells using an anti-cytokeratin

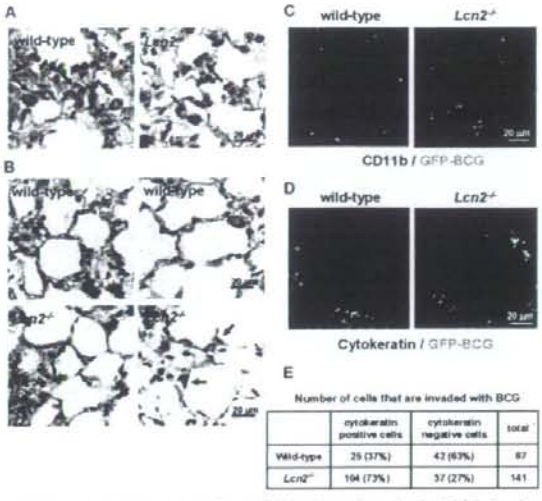

	cytokeratin positive cells	cytokeratin negative cells	total
Wild-type	25 (37%)	42 (63%)	67
Lcn2$^{-/-}$	104 (73%)	37 (27%)	141

FIGURE 4. Increased numbers of *M. tuberculosis* in *Lcn2*$^{-/-}$ alveolar epithelial cells. *A* and *B*, Wild-type and *Lcn2*$^{-/-}$ mice were intratracheally infected with *M. tuberculosis* H37Ra. At 5 days after infection, the lungs were fixed in paraffin, sectioned, and stained with the Ziehl-Neelsen method. Arrows indicate red-stained *M. tuberculosis*. *C–E*, At 5 days after intratracheal infection with GFP-expressing BCG (green), lung tissue sections were stained with anti-CD11b Ab (*C*, red) or anti-pan-cytokeratin Ab (*D*, red), and visualized by fluorescence microscopy. The number of cells containing BCG was counted in a total of ten areas of pictures that visualized different fields (*E*).

Ab indicated that increased numbers of alveolar epithelial cells in *Lcn2*$^{-/-}$ mice contained GFP-expressing BCG compared with those in wild-type mice (Fig. 4, *D* and *E*). Thus, in the absence of Lcn2, invasion and replication of mycobacteria in alveolar epithelial cells were increased.

Therefore, we assessed the sensitivities of alveolar macrophages and alveolar epithelial cells to in vitro infection with BCG. First, alveolar macrophages were isolated from wild-type and *Lcn2*$^{-/-}$ mice, and infected with BCG (Fig. 5*A*). The CFU titers of BCG in macrophages at 4 and 7 days after infection were comparable between wild-type and *Lcn2*$^{-/-}$ cells. Thus, the absence of Lcn2 did not affect the anti-mycobacterial activity in alveolar macrophages. Next, we established AECs from wild-type and *Lcn2*$^{-/-}$ mice. Because AECs are difficult to culture in vitro, we took advantage of transgenic mice harboring a temperature-sensitive mutation of the SV40 large tumor Ag gene under the control of an IFN-γ-inducible H-2K^b promoter element (30–32). Using these mice, we successfully established wild-type and *Lcn2*$^{-/-}$ AECs, both of which were stained with anti-SP-C Ab (data not shown). AECs from wild-type mice expressed Lcn2 mRNA and secreted Lcn2 protein into the culture medium when infected with BCG (data not shown). Thus, these AECs showed the characteristics of type II alveolar epithelial cells. AECs were infected with BCG, and the CFU titers within the cells were counted at 1, 2, 3, and 4 days after infection (Fig. 5*B*). At 3 and 4 days after infection, the CFU titers in *Lcn2*$^{-/-}$ cells were increased compared with those in wild-type cells. Addition of exogenous rLcn2 reduced the CFU numbers in *Lcn2*$^{-/-}$ cells (Fig. 5*C*). Taken together, these findings indicate that the high susceptibility of *Lcn2*$^{-/-}$ mice to *M. tuberculosis* infection is attributable to impaired clearance of mycobacteria from alveolar epithelial cells, rather than alveolar macrophages, in the absence of Lcn2.